https://doi.org/10.5194/egusphere-2026-887
Preprint. Discussion started: 9 April 2026

GOFS16: an operational global ocean analysis and forecasting system at eddy-resolving resolution

Simona Masina[1], Andrea Cipollone[1], Doroteaciro Iovino[1], Stefania Ciliberti[1*], Rita Lecci[1], Sergio Cretí[1], Vladyslav Lyubartsev[1], Giovanni Coppini[1], Emanuela Clementi[1]

[1] CMCC Foundation- Euro-Mediterranean Center on Climate Change, Italy

*now at Nologin Oceanic Weather Systems, Spain

Correspondence to: Simona Masina (simona.masina@cmcc.it)

Abstract. The Global Ocean Forecast System GOFS16 is an operational ocean analysis and forecast system that has been running daily at the Euro-Mediterranean Center on Climate Change since early 2017. GOFS16 produces 6-day forecasts of the state of the global ocean and sea ice (three-dimensional ocean temperature, salinity, and currents, as well as sea level, sea ice thickness, concentration and drift) with a system based on the NEMO model configured in a global eddying ocean at 1/16° horizontal resolution and 98 vertical levels. To compute the initial conditions for the forecasting, in situ observations of temperature and salinity, altimeter data of sea level anomaly and satellite sea surface temperature fields are jointly assimilated each day over a 1-day observation window with a 3DVar scheme, OceanVar, adapted to handle the global high-resolution grid. This paper introduces the first version of the GOFS16 system and describes its components and the validation procedure, which routinely produces statistics of the system skill. The scientific assessment is presented for the period January 2022-December 2023, at global and regional scales. Results indicate that GOFS16 performs within the expected range of skill for current global systems. However, the impact of the eddy-resolving resolution is hidden either by system weaknesses or traditional verification metrics not adequate at such resolution.

1. Introduction

The unique capability of satellite altimetry to observe the global ocean in near-real-time at high resolution (Le-Traon et al., 2017) and the development of the Argo program were essential to the establishment of global operational oceanography (Wong et al., 2020). Building on recent advances in computational resources, several national centers have developed ocean analysis and forecasting systems that operate on global scales and provide estimates of the mesoscale dynamics using eddy-permitting and eddy-resolving models (e.g., Blockey et al., 2014; Liu et al., 2021; Lellouche et al., 2018; Garraffo et al., 2020; Smith et al., 2016; Brassington et al., 2012). The Global Data Assimilation Experiment (GODAE, 1998–2008) was phased with the T/P and ERS-1/2 successor missions (Jason-1 and ENVISAT) and was instrumental in advancing global ocean analysis and forecasting capabilities (Smith and Lefebvre, 1997; Tonani et al, 2015; Shiller et al., 2018). The development of an integrated approach, combining satellite and in situ observations with numerical models, has been fundamental and fostered a series of major achievements in oceanography. At the same time, the ocean modelling community started to address the challenges that the need to resolve complex mesoscale dynamics poses and nowadays global models capable of realistically representing the full dynamics and life cycle of baroclinic eddies, at least over most of the entire global domain, are becoming increasingly widespread (e.g. Chassignet et al., 2020). However, despite the significant improvements in model development (Fox-Kemper et al., 2019), computational capacity and the increased availability of observations during the last two decades (Sloyan et al., 2018; Davidson et al., 2019), one among the original goals of the global operational community has not been reached completely, that is the eddy-resolving capacity in the continental shelf

https://doi.org/10.5194/egusphere-2026-887
Preprint. Discussion started: 9 April 2026

regions and at high polar latitudes where resolution higher than 1/10° are needed to resolve the dominant eddies scales (Hallberg, 2013). In the attempt to close this gap and bring the global forecasting capabilities also in regions which are nowadays only served by regional systems, CMCC developed GLOB16, a global eddy-rich configuration of the ocean and sea ice system (Iovino et al., 2016). GLOB16 is based on the state-of-the-art modelling framework NEMO (Nucleus for European Modelling of the Ocean, Madec et al., 2013) and reaches a horizontal grid spacing of ~3km in polar regions and can resolve mesoscale features over most of the global ocean. It is worth noting that an evaluation of a set of numerical experiments following the Ocean Modeling Intercomparison Protocol (OMIP) and using increasing resolution global configurations of NEMO indicates that the eddying 1/16° configuration (GLOB16) improves the representation of the boundary currents and transports through key straits, in addition to a more energetic oceanic state and enhanced mesoscale variability (Iovino et al., 2023). These results support the feasibility of GLOB16 as a modelling tool for a forecasting system prone to serve activities such as maritime transportation, search and rescue, and emergency operations due to oil dispersion accidents.

GLOB16 was successfully coupled to a 3D variational assimilation scheme called OceanVar (Dobricic and Pinardi, 2008) used to provide the initial conditions for ocean forecasting. The assimilation method has been extensively and successfully used at CMCC in regional forecasting systems (Coppini et al., 2023; Ciliberti et al., 2022), as well as in global eddy-permitting reanalyses implementations (Storto et al. 2016a; Storto et al. 2016b; Masina et al. 2017) and has been recently adapted to deal with large amount of data through a hybrid-parallelization scheme (Cipollone et al., 2020).

Since mid 2017, and thanks to the demonstrated capacity of GLOB16 to accurately simulate mesoscale dynamics, a new global eddying analysis and forecasting system GOFS16 (Global Ocean Forecasting System at 1/16 resolution) has been designed and implemented at CMCC and currently running in operational model. The 5-day-long forecast product of GOFS16 includes hourly/daily frequency data for the 3D temperature (T), salinity (S), meridional/zonal velocity (V/U), as well as 2D sea surface height (SSH). Sea ice properties are also available. A dedicated web application (https://gofs.cmcc.it) offers to users daily bulletins of GOFS16 product catalogue through 2D maps of forecasted variables. Additionally, it displays GOFS16 metrics where GOFS16 best estimate fields are compared to available in-situ temperature and salinity profiles from the Copernicus Marine Service.

The forecast skill of the model is routinely monitored by producing different types of statistics. The root-mean-square error (RMSE), anomaly correlation and climatological skill score are calculated for both SSH and sea surface temperature (SST) as well as for three-dimensional T and S. The statistics are calculated for the global domain as well as numerous sub-regions of the world ocean.

This paper is organized as follows: in Section 2, we present the GOFS16 in its three components (model, data assimilation and assimilated observations). In Section 3, the operational chain is described, while Section 4 illustrates the validation framework used to monitor the analysis and forecast skills of the system. Finally, in Section 5 we summarize the main results and provide some hints for future developments.

2. Description of the GOFS16 system

GOFS16 is built upon 3 main numerical components:

a) the ocean and sea ice general circulation model, based on the NEMO framework (Madec et al., 2013), at 1/16° horizontal resolution and 98 vertical levels;

b) a three-dimensional variational (3DVar) data assimilation scheme OceanVar, (Dobricic and Pinardi, 2008) that assimilates in situ Temperature (T) and Salinity (S) profiles and satellite Sea Level Anomaly (SLA) and Sea Surface Temperature (SST) observations;

https://doi.org/10.5194/egusphere-2026-887
Preprint. Discussion started: 9 April 2026

c) a nudging scheme that uses space-borne SST observations and Sea Ice Concentration (Huang et al, 2020, Reynolds et al., 2007) supplied by the National Oceanic and Atmospheric Administration (NOAA), and Sea Surface Salinity (Good et al., 2013).

2.1. Physical model

The global ocean/sea ice configuration consists of the NEMO ocean model (version 3.4), that integrates numerically primitive equations and a non-linear equation of state with variables distributed on a three-dimensional Arakawa C grid. GOFS16 is based on the CMCC global eddy-rich configuration (GLOB16) whose detailed description and validation are presented in Iovino et al. (2016).

GOFS16 core model uses a quasi-isotropic tripolar grid with a 1/16° horizontal resolution, corresponding to 6.9 km at the Equator, increasing toward high latitudes with approximately 3 km in polar regions. The vertical coordinate system is based on 98 fixed geopotential levels, where the level thickness is a double *tanh* function of depth such that the level spacing varies from approximately 1m near the surface to 160m in the deep ocean. Partial cell parameterization is used to better represent the topographic flow (Barnier et al., 2006). The model bathymetry is a combination of 3 interpolated products: ETOPO2 (for the deep ocean; US Department of Commerce, 2006), GEBCO (over the continental shelves shallower than 300 m; IOC, IHO and BODC, 2003) and Bedmap2 (south of 60° S; Fretwell et al., 2013). Hand-editing in key areas such as channels and small islands removed the remaining bathymetry artifacts.

A linearized free-surface formulation is used (Roullet and Madec, 2000) and a free-slip lateral friction condition is applied at the lateral boundaries. The momentum advection term is computed with the energy and enstrophy conserving scheme by Arakawa and Lamb (1981). A lateral isopycnal diffusion on tracers (80 $m^2\ s^{-1}$ at the Equator and decreasing poleward, proportionally to the grid size) and a biharmonic lateral diffusion on momentum (-0.5 x 10^{10} $m^4\ s^{-1}$ at the Equator and decreasing poleward as the cube of the grid size) are used. The advection of the tracers (temperature and salinity) is computed with a total variance dissipation scheme (Zalesak, 1979) to avoid the problem of overshooting where sharp gradients exist in the tracer fields (Lévy et al., 2001). Vertical mixing is parameterized using the Turbulent Kinetic Energy (TKE) turbulent closure scheme (Blanke and Delecluse, 1993), which includes the effect of Langmuir cell circulation (Axell, 2002) and surface wave breaking energetics (Mellor and Blumberg, 2004). Unresolved vertical mixing processes are represented by vertical eddy diffusivity and viscosity coefficients of 1.2×10^{-5} $m^2\ s^{-1}$ and 1.2×10^{-4} $m^2\ s^{-1}$, respectively. Vertical eddy mixing of both momentum and tracers is enhanced in case of static instability. The turbulent closure model does not apply any specific modification in ice-covered regions. Bottom friction is quadratic, and a diffusion bottom boundary layer parameterization is used for temperature and salinity tracers.

Momentum and heat turbulent surface fluxes are prescribed to the model using the bulk formulae of Large and Yeager (2004), using fields provided by National Centers for Environmental Prediction (NCEP) operational Global Forecast System (NCEP GFS, 2026), on a 0.25° by 0.25° global latitude-longitude grid. The turbulent variables are applied at a 6 hourly frequency and radiative and freshwater fluxes are daily fields. In the present configuration, we use absolute wind stress, so the ocean surface current is not included in the bulk formula calculations for surface fluxes. Shortwave penetration is applied through the RGB (red-green-blue) formulation that splits the visible light into three wavebands, modulated by a constant and uniform chlorophyll value.

A monthly runoff climatology, derived from Dai and Trenberth (2009) for river input and Jacobs et al. (1992) for Antarctica ice sheet melting, is applied along the land mask. The freshwater is added to the surface, assumed to be fresh and at local SST. As the thickness of the uppermost level is 0.4 m, diurnal cycle is imposed on solar flux: the daily averaged short-wave flux is spread over the day according to time and geographical position (Bernie et al., 2007). The mean sea level is free to drift.

https://doi.org/10.5194/egusphere-2026-887
Preprint. Discussion started: 9 April 2026

The ocean model is coupled to the Louvain-la-Neuve sea ice model (LIM2, Fichefet et al., 1997), which includes the representation of both the thermodynamic and dynamic processes. LIM2 features a single sea-ice category and open water represented using ice concentration, a 3-layer thermodynamics with a virtual reservoir of shortwave radiation heat which parameterizes brine inclusions, and implements snow-ice formation by infiltration and freezing of seawater into snow when deep enough. The effect of sub-grid-scale snow and ice thickness distributions is implicitly parameterized by enhancing the conduction of heat through the ice and by melting the ice laterally to account for thin ice melting. The surface albedo depends on the state of the surface (frozen or melting), the snow depth and ice thicknesses (Shine and Henderson-Sellers, 1985). The ice dynamics are calculated according to external forcing (wind stress, ocean stress, and sea surface tilt) and internal ice stresses using C-grid formulation (Bouillon et al., 2009). The elastic-viscous-plastic rheology formulation is applied (Hunke and Dukowicz, 1997), and advection is represented with the second-order moment-conserving advection scheme of Prather (1986).

2.2. Data assimilation scheme and assimilated observations

The data assimilation (DA) component of GOFS16 is called OceanVar, which belongs to the family of three-dimensional variational (3Dvar) analysis systems specifically designed for oceanographic applications (Dobricic and Pinardi, 2008; Storto et al., 2011, 2014). OceanVar has been widely and successfully employed in several global eddy-permitting ocean reanalysis products and their later updates, such as C-GLORS (Storto et al., 2016a, 2016b) and historical ones (CHOR, Yang et al., 2017) and is hereby extended to operate on 1/16° resolution grid. OceanVar solves the preconditioned minimization problem with an incremental algorithm (Courtier, 1997). Specifically, the variational problem consists in the minimization of a cost function J through a Control Variable Transformation (CVT) that defines a space where the errors of the new transformed variables are uncorrelated, and their error covariance matrix simplifies to the identity matrix **(I)**:

$$J[\boldsymbol{v}] = \frac{1}{2}\boldsymbol{v}^T\mathbf{I}\boldsymbol{v} + \frac{1}{2}(\mathbf{H}\,\mathbf{V}\boldsymbol{v} - \boldsymbol{d})^T\mathbf{R}^{-1}(\mathbf{H}\,\mathbf{V}\boldsymbol{v} - \boldsymbol{d}) \quad (1)$$

where $\boldsymbol{v}$ is the new control state defined starting from the distance between analysis and background state $\boldsymbol{\delta x} = \boldsymbol{x} - \boldsymbol{x}^b = \mathbf{V}\,\boldsymbol{v}$ with the preconditioner $\mathbf{V}$ corresponding to the (left) square root of background-error covariance matrix $\mathbf{B} = \mathbf{V}\mathbf{V}^{\mathrm{T}}$; $\mathbf{R}$ is the observation error covariance matrix while the vector of observation departures (or innovations) is $\boldsymbol{d} = \boldsymbol{y} - \mathrm{H}[\boldsymbol{x}^b]$. Note that while the tangent-linear version of observation operator $\mathbf{H}$, evaluated in $\boldsymbol{x}^b$, is employed in J, its full non-linear expression H is used to shape $\boldsymbol{d}$. In OceanVar, the CVT matrix $\mathbf{V}$ provides also a way to model $\mathbf{B}$ without explicitly construct the matrix and is designed through a set of subsequent transformations, $\mathbf{V} = \mathbf{V}_\eta\,\mathbf{V}_h\,\mathbf{V}_v$ whose inverse V^{-1} transforms the increments δx into the new control state $\boldsymbol{v} = \mathbf{V}_v^{-1}\,\mathbf{V}_h^{-1}\,\mathbf{V}_\eta^{-1}\,\boldsymbol{\delta x}$ projecting the errors onto orthogonal uncorrelated modes. The operators in $\mathbf{V}$ are designed to account for vertical covariances ($\mathbf{V}_v$), horizontal correlations ($\mathbf{V}_h$) and sea-level operator ($\mathbf{V}_\eta$). The $\mathbf{V}_\eta$ corresponds to the dynamic height operator (Cooper and Haines, 1996) and evaluates the sea level increment from increments of temperature and salinity by means of a local hydrostatic balance (Storto et al, 2011). In the current implementation, the model state variables consist of three-dimensional temperature and salinity only, i.e. no explicit correction to the sea level anomaly are given. $\mathbf{V}_v$ consists of 25-mode seasonal bivariate vertical EOFs of temperature and salinity estimated from the Eigen-decomposition of anomalies with respect to long-term mean, in a non-assimilative simulation, as in Bellucci et al. (2007). The operator $\mathbf{V}_h$ models horizontal Gaussian covariances by means of an application of a first-order recursive filter with locally varying correlation length-scales. The latter were estimated from the dataset of anomalies of temperature and salinity as in Storto et al. (2014).

https://doi.org/10.5194/egusphere-2026-887
Preprint. Discussion started: 9 April 2026

In the present configuration, the dataset assimilated are listed in Table 1. The associated observation-error covariance matrix **R** is assumed diagonal, i.e. observation errors are assumed independent. For in situ observations, the error depends on the specific variable (temperature, salinity), the depth and location, the instrumental accuracy and representativeness error. For sea level anomaly, the error variance accounts for the satellite instrumental accuracy, the mean dynamic topography error (provided by CLS/AVISO) and the representativeness error (Storto et al., 2011).

Table 1 Assimilated dataset in the variational scheme

Data type	Data source
T/S profiles	Near-real-time vertical profiles of temperature and salinity from Argo, XBTs and CTDs, etc, disseminated by Copernicus Marine Service INSITU TAC INSITU_GLO_NRT_OBSERVATIONS_013_030, (2026)
SLA	Near-real-time satellite along-track data disseminated by Copernicus Marine Service SL-TAC SEALEVEL_GLO_PHY_L3_NRT_008_044, 2026), SEALEVEL_GLO_PHY_L4_NRT_008_046, (2026)
SST	Satellite retrievals from Metop-B/AVHRR (EUMETSAT/OSI SAF, 2016) and GCOM-W/AMRS-2 (Remote Sensing System, 2017) distributed by NOAA

SLA observations are treated using a simple spatial bias correction procedure based on the statistics of the innovation $\bar{\boldsymbol{d}}$ for seven days. The bias $\bar{\boldsymbol{d}}$ is multiplied by a factor $\left(\frac{\sigma_\eta^2}{\sigma_\eta^2+\sigma_O^2}\right)\left(\frac{\bar{d}^2}{\bar{d}^2+\sigma_\eta^2}\right)$ that goes between [0-1] and reduces its value by comparing the variability of the model and observations. The first term is the ratio between model standard deviation $\boldsymbol{\sigma}_\eta^2$ and the sum of observation $\boldsymbol{\sigma}_O^2$ and model one. The second term compares the bias with the model variability. If $\boldsymbol{\sigma}_O^2 \gg \boldsymbol{\sigma}_\eta^2$ than observations are not reliable, and the bias is reduced to zero. The same happens in the case the variability is much larger than the square bias ($\boldsymbol{\sigma}_\eta^2 \gg \bar{\boldsymbol{d}}^2$). Such unbias scheme is applied at validation step as well. No unbias is instead performed yet on the SST data, despite some literatures have proven it as beneficial (Blockley et al., 2014). SST observations are assumed to be located at the shallowest model level. The associated errors employed is provided together with the data. A lower-bound for SST error (0.3°C) is included to reduce strong warming or cooling of the water column generated by an over-confidence in the observations.

Thinning and background quality checks are implemented during the assimilation step. The background quality check rejects observations whose departure from the corresponding model-counterparts exceed three times the sum of the observational and background-error variances. The data thinning procedure handles multiple independent observations of the same type that occur in the same grid cell. In that case, only the observation closest in time to the middle of the assimilation window is retained. In the vertical, we implemented a conservative check for Argo profiles: if an observation is flagged as bad, then all deeper observations are excluded from the same profile. This last procedure removes observations that could potentially generated spurious large increments at depth being wrongly reported as good ones. The OceanVar scheme has specification of background- and observation-error variances as in Storto et al. (2016b). Background-error correlation length-scales have been scaled to the 1/16° resolution from the 1/4° resolution configuration (ORCA025 grid).

The analysis scheme of GOFS16 includes a nudging scheme to correct the surface heat and freshwater fluxes. The dataset employed to constrain the heat flux is the gridded sea-surface temperature analyses provided by NOAA that uses infrared retrievals from AVHRR instruments, drifter and buoy in-situ measurements (Reynolds et al., 2007). The relaxation time scale is 15 days. Alongside, the fresh-water flux is corrected through the sea-surface salinity product of the UK MetOffice EN4 (Good et al., 2013) objective analyses, with a relaxation time scale of 300 days. As an important step forward for the prediction of sea and sea-ice states at high latitudes, GOFS16 also implements a univariate data assimilation scheme for sea-ice concentration, ingesting optimal-interpolated daily field from NOAA delivered together with the SST-OI field. The assimilation scheme consists of nudging to the sea-ice analysis with an 8-hour relaxation time-scale.

https://doi.org/10.5194/egusphere-2026-887
Preprint. Discussion started: 9 April 2026

The GOFS16 system is designed to share the same grid, 1/16°, at any step. This brought several benefits starting from a direct ingestion of DA corrections into the model run without the need of extra interpolation that could lead to additional errors. Moreover, it helps the system to maximize the amount of information coming from high-resolution observational networks and to reduce the artificial spatial correlation among observations that are inevitably introduced at the length scale of grid spacing. While the model resolution is primarily linked to the scale of the physical processes that can be expicitally resolved or sustained, the assimilation resolution goes to shape the representativeness error for observations that are dense with respect to the grid. This is particularly true for the assimilation of SST observations when the employment of a coarser grid inevitably worsens the quality of the final production. The benefits of using the same resolution for both model dynamics and DA, versus the alternative one in which the ocean output was interpolated onto 1/4° horizontal resolution grid as first guess fields for OceanVar, have been shown in Cipollone et al. (2020).

3. Operational implementation and daily running

GOFS16 production of the day *T* starts the day before, with a workflow manager downloading and preprocessing both observations and boundary forcing around *T*-4h (i.e., previous day around 8 p.m.). After the full production is accomplished, several variables (Temperature, Salinity, Ocean Currents, Sea Level, Ice Concentration, etc.) at different days are inspected before the dissemination in the late morning of day *T*.

The cycle of model integrations and corrections for the production day *T* begins 48h ahead with a first ocean simulation from *T*-48h to *T*-24h that provides a "first guess" field to the DA system. The OceanVar system then assimilates the observations available at the same time window and generates increments to correct the ocean state. A second simulation again from *T*-48h to *T*-24h is performed where the corrections from DA system are incorporated with an incremental analysis update (IAU) that spreads such corrections over the full day. The final output of this second simulation is referred to as "best estimate", representing the most accurate reconstruction of the ocean state between *T*-48h and *T*-24h. Between *T*-24h and *T* a simulation is then produced representing the starting point of the forecast integration. We extend the definition of hourly nowcast (https://wmo.int/media/magazine-article/nowcasting-guidelines-summary) to daily nowcast, indicating such the model output between *T*-24h to *T*. A detailed description of each step of the operational chain is described below and shown in Fig.1.

Figure 1: Schematic representation of the daily operational cycle of the GOFS16 forecasting system.

https://doi.org/10.5194/egusphere-2026-887
Preprint. Discussion started: 9 April 2026

The download and pre-processing of observations and boundary forcing is handled by a Python-based workflow management system, that performs the following tasks:

- The download of available in-situ and satellite observations as needed for running the DA scheme within the time interval (T-48h, T-24h) from multiple data sources (Table 1)
- The download of daily atmospheric analysis fields from the NCEP Global Forecasting System, at 0.25 deg spatial resolution and 6-hourly temporal frequency from T-48 h up to T-12h and followed by forecast fields out to T+156 h. The atmospheric variables used by the system are defined by the CORE bulk formulae forcing method (Large and Yeager, 2004): 2m specific humidity, 2m air temperature, 10m wind velocity, total precipitation, snow fall and radiative fluxes at sea surface (short and long wave radiation). For the period [T-48h, T-24h], the optimally interpolated observation-derived SST and SSS maps (see Section 2) are also downloaded to correct the ocean state through nudging schemes. A *Sea-Over-Land* extrapolation method (De Dominicis et al., 2014) is applied along the coastline of each map to eliminate possible inconsistencies with the model sea-land mask and reducing boundary effects in the atmospheric forcing.

Once the datasets are pre-processed, the workflow manager starts the model-DA cycle:

- A 24-hour NEMO model simulation is run for the period T-48h to T-24h to generate the daily first-guess field ready for the assimilation.
- The OceanVar system bilinearly interpolates the first-guess field to the observation positions, producing the corresponding misfits that are used to initialize the minimization and generate the final daily increments (Cipollone et al., 2020). The OceanVar system assimilates only observations that are flagged as "good" in the observational datasets after the background quality check and thinning procedure (as discussed in the dedicated section).
- The model is then integrated a second time for the same time-period (T-48h to T-24h) with the DA increments added to the restart of the model with an incremental analysis update (IAU) algorithm. The final model outputs, saved as "best estimate", serves as the restart of the nowcast (T-24h-T) used to initialize the forecast run.
- The system runs in hindcast mode from T-24h to T and in forecasting mode from T to T+156h. At the time of the data download (T-4h) for the production day T-24h, some in-situ observations are already available for the interval T-24h to T-4h. As a potential further improvement, an additional cycle of simulation/assimilation could be added in the future to assimilate these available in-situ data, provided that their inclusion demonstrates a significant benefit to the forecasting skill score.

The forecast datasets are produced at hourly and daily frequency and then post-processed for the dissemination to end-users. All the tasks are run on the CMCC HPC Data Center, based on a Lenovo SD630 v2 computing system that embeds Intel Xeon Platinum 8360Y (36 cores) multi-CPU with a total number of 12.240 cores. OceanVar runs on 900 cores, while the NEMO ocean-sea ice model runs on 1.620 cores, employing about 0.33 wall clock hours for producing a complete daily cycle of assimilation and forecast. It generates approximately 280 GB of output files per cycle.

4. Evaluation of best estimate/forecast skill

The best estimate and forecast skill of the system is routinely monitored and involves different validation and verification processes: from the simple daily inspection of core variables (temperature, salinity, etc.) to the evaluation of several statistical metrics. GOFS16 best estimate performance is validated through a web-based validation tool which makes the

https://doi.org/10.5194/egusphere-2026-887
Preprint. Discussion started: 9 April 2026

comparison against quality-controlled in-situ observations provided by ARGO float profiles, mooring buoys and tide gauges, computing statistical metrics and quality indicators. The tool uses freely available near-real-time in-situ temperature and salinity profiles INSITU_GLO_NRT_OBSERVATIONS_013_030 (see Table 1 for reference) from the Copernicus Marine Service In Situ Thematic Assembling Center (INS TAC) and the EMODnet Physicsdata portal (EMODNET, 2026), which are compared with model equivalent values. The operational routine stores the monthly updated of the dataset. An example of the Graphical User Interface (GUI) is presented in Fig. 2a. The tool allows to select time intervals, depth horizons, and sub-regions, and computes on-the-fly temporal and spatial averages of the model output and observations, as well as mean bias and RMS profiles, and TS-diagrams. The system can calculate the evaluation metrics over any polygonal area specified by the users. An example of such an implementation is shown in Fig. 2b.

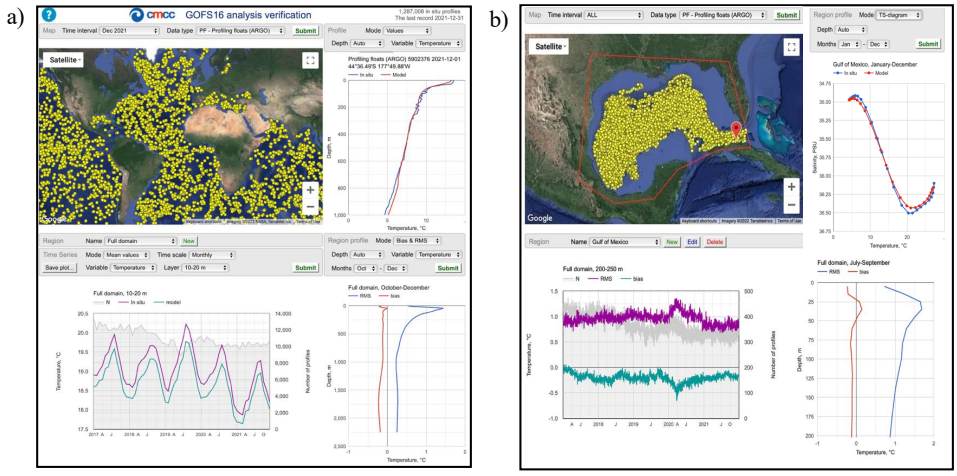

Figure 2: a) Graphical user interface of the GOFS16 best estimate verification tool and an example using Argo profiles. b) Application of the tool to a predefined polygonal area in the Gulf of Mexico. Background Maps ©2022 NASA, *Copyright TerraMetrics, LLC --www.terrametrics.com*.

Thanks to achieved milestones in its operational deployment, since 2021 GOFS16 entered the GODAE/OceanPredict intercomparison exercise that aims to assess and compare the quality of several global operational ocean forecasts, by providing a unique intercomparison framework (Hernandez et al., 2015). A common protocol is set up by the Intercomparison and Validation Task Team (IV-TT) consisting of several pointwise class-4 metrics that are evaluated by co-localizing the model outputs and observations at the time and date of the observations (Ryan et al., 2015). Considering the recent inclusion of GOFS16, there are 7 different global operational systems that have participated in such practice: each system downloads an identical set of observations and shares the model-counterpart for both the best estimate and forecasts. Up to the time of the skill assessment presented here, the Met Office Observation Processing System (OPS) was responsible for assembling and quality checking the in-situ SST, Temperature/Salinity profiles, and altimetry data, which were then shared on the USGODAE servers and are presently on Environment and Climate Change Canada (ECCC) servers. Near-real time temperature and salinity observations are usually extracted from ~500 Argo GDAC daily profiles roughly covering the global ocean with a resolution of 10° × 10°. Satellite SLA and in-situ SST data come from CLS AVISO Level 3 along-track satellite retrievals and in-situ surface drifters with about ~100K and 70K observations available every day, respectively. The class-4 metrics defined in the IV-TT protocol are evaluated both on a global and on a sub-basin level using the definition established in the GODAE-MERSEA framework (Hernandez et al., 2009) and listed in Table 2.

https://doi.org/10.5194/egusphere-2026-887
Preprint. Discussion started: 9 April 2026

Table 2 Ocean sub-basins definition following GODAE-MERSEA framework

Name	Longitude	Latitude
Global Ocean	180W-180E	90S-90N
North Atlantic	100W-31E	0-70N
Tropical Atlantic	70W-30E	20S-20N
South Atlantic	70W-30E	60S-0
North Pacific	100E-77W	0-65N
Tropical Pacific	90E-70W	20S-20N
South Pacific	100E-70W	60S-0
Indian Ocean	20E-120E	40S-31N
Australasia	90E-180E	70S-20N

Three different metrics are used in the validation exercise: RMSE, bias and anomaly correlation coefficient (ACC), whose formulae are the following:

$$BIAS\ (\boldsymbol{X}) = \frac{1}{N}\sum_{a=1}^{N}(\boldsymbol{X}_a - \boldsymbol{O}_a) = \overline{(\boldsymbol{X} - \boldsymbol{O})} \quad (2)$$

$$RMSE(\boldsymbol{X}) = \sqrt{\frac{1}{N-1}\sum_{a=1}^{N}(\boldsymbol{X}_a - \boldsymbol{O}_a)^2} \quad (3)$$

$$ACC(\boldsymbol{X}) = \frac{\sum_{a=1}^{N}(\boldsymbol{X}_a - \boldsymbol{C}_a) - \overline{(\boldsymbol{X}-\boldsymbol{C})}] \cdot [(\boldsymbol{O}_a - \boldsymbol{C}_a) - \overline{(\boldsymbol{O}-\boldsymbol{C})}]}{\sqrt{\sum_{a=1}^{N}(\boldsymbol{X}_a - \boldsymbol{C}_a) - \overline{(\boldsymbol{X}-\boldsymbol{C})}]^2 \cdot \sum_{a=1}^{N}[(\boldsymbol{O}_a - \boldsymbol{C}_a) - \overline{(\boldsymbol{O}-\boldsymbol{C})}]^2}} \quad (4)$$

where indexes a run over the N observation locations, $\boldsymbol{O}$ represents the set of observations, $\boldsymbol{X}_a$ denotes the model value at the observation location, and $\boldsymbol{C}_a$ denotes World Ocean Atlas (2005) monthly climatology interpolated at the observation position and at the day of the observation. The overbar shows the average over the number of observations. The bias quantifies the mean difference between model and observations, RMSE measures the average magnitude of the error, and ACC represents a measure of the correlation between model and observed anomaly with respect to the climatology (following the WMO definition; GDPFS WMO, 2010), after removing the seasonal cycle that could positively impact the correlation.

The evaluation presented in this paper covers the period 1 January 2022 to 31 December 2023, GOFS16 equivalents can be found in https://doi.org/10.5281/zenodo.18504242 (Cipollone, 2026)

, after approximately 4 years since the entrance in service of the operational system. Since its birth, the system has gone through some bug fixing and continuous improvements, supported by the routine daily evaluation of its skills.

4.1 Global and regional SST and SLA

Figure 3a shows the time series of the global average of bias and the RMSE of the SST for the best estimate, the nowcast and forecast days during the 1st January 2022-31st December 2023 period. The nowcast is affected by a cold bias oscillating around -0.1°C, with maximum deviations from the mean during the boreal summer months and with values very similar to those of the best estimate. After five days, the forecast bias approximately doubles on average and shows enhanced

https://doi.org/10.5194/egusphere-2026-887
Preprint. Discussion started: 9 April 2026

variability. From May to August, the RMSE also reaches the highest values with an average of about 0.7°C, while it levels off around 0.5°C during the rest of the year. The best estimate follows a similar time evolution although with slightly lower values in the RMSE. A boreal summer locked skill degradation is common to most operational global systems at lower resolution (Ryan et al., 2015) and it is likely due to the higher ocean surface variability during the season, which peaks in the northern hemisphere since the drifters populate mostly those latitudes.

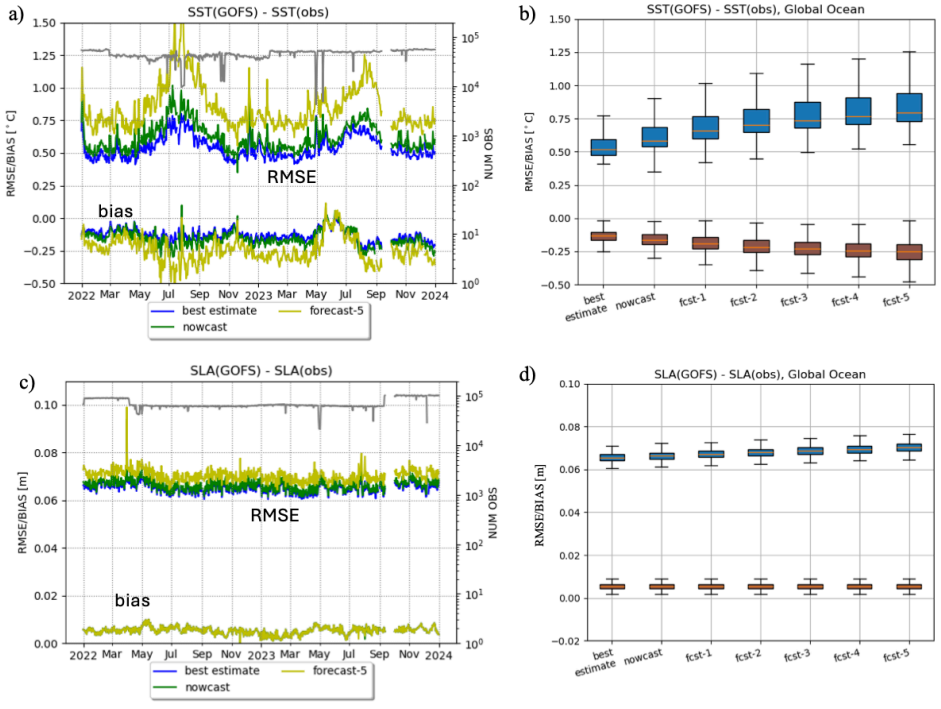

Figure 3: a) Timeseries of SST RMSE and bias for the best estimate (blue line), nowcast (green line) and the sixth day of forecast (yellow). Gray line shows the daily number of observations. b) SST RMSE (blue boxes) and bias (red boxes) distributions for the best estimate, nowcast and each forecast days. c) Same as in panel (a) but for SLA. d) Same as in panel b, but for SLA.

The evolution of the SST bias and RMSE as a function of forecast lead time are shown in Fig. 3b. The orange lines indicate the median values, while the boxes show the interquartile range, and the vertical lines provide the 95th percentile. The bias median values double after three forecast days, moving from the best estimate value of approximately 0.1°C to 0.2°C, after which it increases more slowly. Similarly, the RMSE increasing tendency is maximum during the first three days with a jump of approximately 0.2°C from the initial best estimate error of 0.5°C, but after that it levels off and the median values never exceed 0.8°C.

It is worth noting that the high resolution of the GOFS16 system does not seem to be beneficial for the SST skill with respect to other lower resolution systems (Ryan et al., 2015; Liu et al., 2021) and further investigations are required to understand whether this is the consequence of a double penalty effect (Hoffman et al., 1995; Ebert et al., 2013) or whether it is due to other causes such as the relative coarse atmospheric forcing used in GOFS16, or a possible inconsistency between the assimilated SST observations and the surface heat flux adjustment, which uses nudging to a different SST product. An on-going activity with an updated version of NEMO and higher-resolution ECMWF atmospheric forecast is under way and the preliminary results tend to suggest a general beneficial impact on the large-scale patterns in SST and surface currents. The best estimate spatial pattern of bias and RMSE (Fig. 4) show that the highest values are localized in mesoscale active regions,

https://doi.org/10.5194/egusphere-2026-887
Preprint. Discussion started: 9 April 2026

in the Arctic region and, more suspiciously, in the North Pacific in the 30-60°N latitude band, where it is evident the most critical skill degradation in the nowcast (not shown).

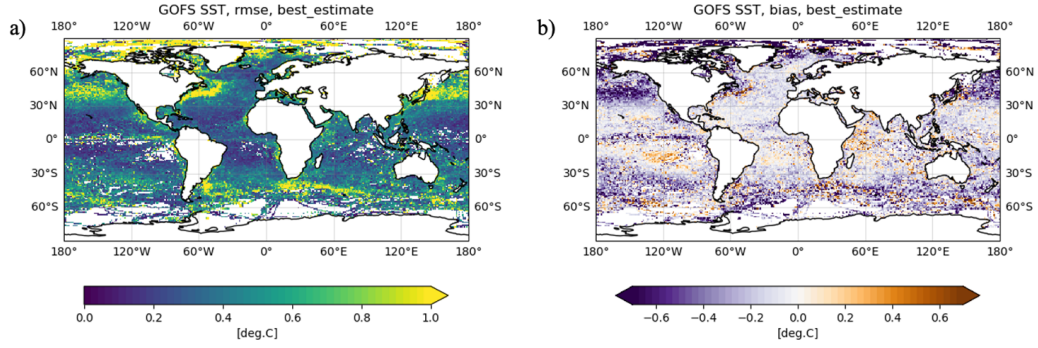

Figure 4: Spatial distribution of (a) RMSE and (b) bias of the SST for the GOFS16 best estimate over the period January 2022-December 2023.

The two bottom panels of Fig. 3 are the equivalent of the upper panels but for SLA. Excluding high frequency small oscillations, both the mean bias and RMSE are constant in time, always below 0.01m (after the bias removal) and 0.07m, respectively. There is no evident degradation from the best estimate to the nowcast in both metrics and at longer forecast days there is only a slight decrease of approximately 0.01m in the system RMSE while the bias remains constant at increasing forecast lead time (Fig.3c). It is interesting to note that the GOFS16 SLA skill falls within the range of the best forecast systems (Ryan et al., 2015; Blockley et al., 2014) suggesting that the SLA, differently from the SST, is not affected by possible counteracting effects deriving from the higher resolution and the not optimal atmospheric forcing. The bias and RMSE spatial patterns of the SLA confirm that the only regions where there is an evident increase of these values are the mesoscale rich regions both in the best estimate (Fig. 5) and nowcast (not shown) with barely any differences among them. The regional performance of the GOFS16 best estimate (Fig.6) is examined using the regions defined in Table 2. Results confirm that all the regions are affected by a cold SST bias and a positive SLA bias (except for the South Atlantic).

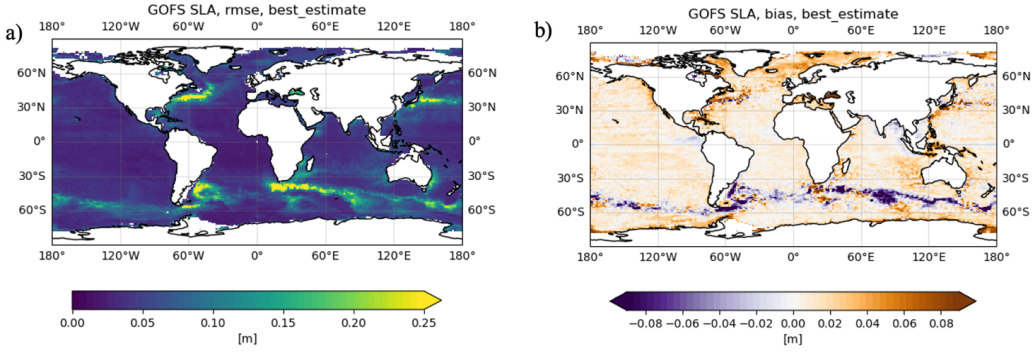

Figure 5: a) Spatial distribution of (a) RMSE and (b) bias of SLA for the GOFS16 best estimate over the period January 2022-December 2023.

https://doi.org/10.5194/egusphere-2026-887
Preprint. Discussion started: 9 April 2026

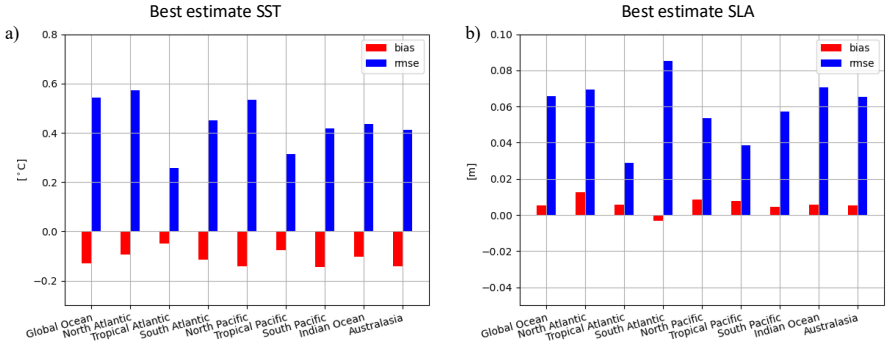

Figure 6: Regional RMSE (blue) and bias (red) for (a) SST and (b) SLA.

The North and the South Pacific subregions have the highest SST bias, while the tropical Atlantic shows the minimum bias. For the RMSE, the North Atlantic and the North Pacific show the highest values in SST, while the tropical regions of both oceans have the lowest values for both SST and SLA. The South Atlantic is characterized by the minimum SLA bias, largely due to compensating effects in the Antarctic Circumpolar Current region (Fig.5b), but also by the maximum RMSE due to high errors in the Agulhas and Malvinas eddy-rich regions (Fig.5a). Overall, the regional analysis agrees with the general findings from other global forecasting systems (Ryan et al., 2015; Liu et al., 2021) and confirms the better forecast skills in the tropical regions for both SST and SLA.

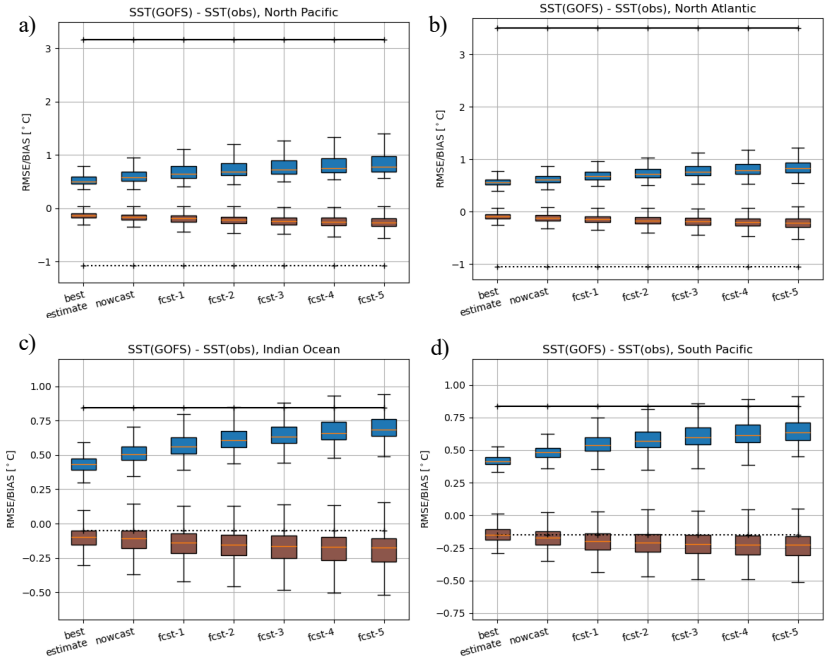

Figure 7: SST RMSE (blue boxes) and bias (red boxes) distribution for the best estimate, nowcast and forecast days for the (a) North Pacific, (b) North Atlantic, (c) Indian Ocean, and (d) South Pacific. Black lines show the climatological reference for RMSE (solid line) and bias (dotted line).

In addition to the calculation of the forecast errors, GOFS16 skill scores are also compared against climatology, that consists of the temporally interpolated monthly SST climatologies based on the objective analysis at 1/4° applied to World Ocean Database 2001(Boyer et al., 2005) and provided by the Met Office Observation Processing System (OPS) .

https://doi.org/10.5194/egusphere-2026-887
Preprint. Discussion started: 9 April 2026

In terms of RMSE, forecasts consistently outperform are climatology at global and regionally scales (Fig.7, for simplicity only four regions are shown: North Pacific, North Atlantic, Indian Ocean, South Pacific) with a more evident positive performance in the Northern Hemisphere (both Atlantic and Pacific Oceans), while in the tropical regions and the Southern basins the differences between the climatology and forecast errors tend to converge as the forecast lead time increases. The cold SST bias evolves similarly across regions with similar amplitudes and distributions. Such bias can be probably related either to the assimilation of SST or to the external atmospheric forcings, and clearly needs to be further investigated and improved. To this end, unbias procedures have been widely used in literature for assimilating SST (Barbosa et al., 2024; Mignac et al., 2025) and are presently under-development for GOFS16 (Broccoli and Cipollone, 2025).

The regional evolutions of RMSE and bias for SLA, as well as their error distributions, are shown in Fig. 8 for the same four regions. The degradation of SLA skill with forecast lead time is lower than for SST, consistent with other systems (Ryan et al., 2015).

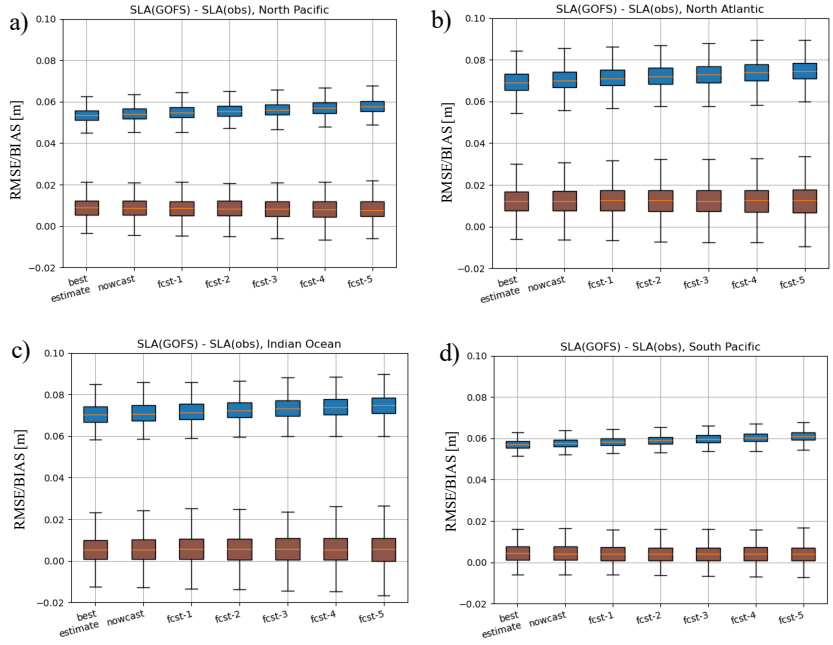

Figure 8: a) SLA RMSE (blue boxes) and bias (red boxes) distribution for the best estimate, nowcast and forecast days for the (a) North Pacific, (b) North Atlantic, (c) Indian Ocean, and (d) South Pacific.

4.2 Global and regional subsurface temperature and salinity

The 0-1500m subsurface temperature and salinity bias and RMSE are evaluated against the in-situ observations, mainly ARGO floats data. Like SST, also the subsurface temperature has a cold bias of approximately 0.1°C, but differently form the SST, it does not show a summer amplification (Fig.9a) nor a clear dependence on forecast lead time (Fig.9b). The RMSE has a significant increase at nowcast (from 0.71°C to 0.87°C), but after that it is quite constant in time rising to 0.92°C at the last day of forecast.

https://doi.org/10.5194/egusphere-2026-887
Preprint. Discussion started: 9 April 2026

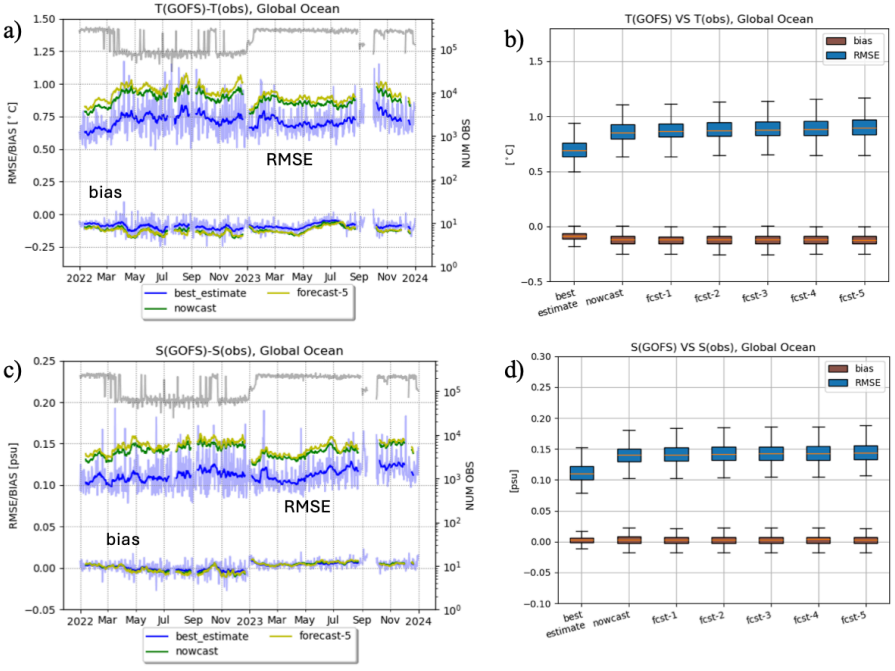

Figure 9: a) Timeseries of model versus in-situ temperature RMSE and bias vertically integrated between 0-1500m for the best estimate (blue line), nowcast (green line) and the fifth day of forecast (yellow). Blue shade corresponds to daily values, while thick lines show the 2-week running mean. Gray line labels the daily number of observations. b) SST RMSE and bias distribution for the best estimate, nowvast and forecast days. c) Same of a) but for salinity. d) Same of b) but for salinity.

The subsurface salinity bias oscillates around the zero value for the best estimate as well as for the whole forecast cycle, with only a slight increase in the interquartile range (Fig.9d). Similarly to the subsurface temperature, the salinity RMSE shows the only significant increase at nowcast and then it remains constant with the median values always below 0.15 psu (Fig.9c). It is worth noting that, based on this analysis, GOFS16 appears to perform better than other lower resolution forecast systems in terms of subsurface salinity (Ryan et al., 2015; Liu et al., 2021) and it is comparable for the subsurface temperature. However, these findings stem only from a first qualitative assessment. A robust and accurate intercomparison across systems should be carried out using identical reference observations and a consistent methodology to calculate metrics.

The cold bias affecting the subsurface temperature is maximum around a depth of 30m while the RMSE reaches the highest value below, suggesting a diversified source of problems causing a colder temperature mean state (Fig.10a). The position of the cold bias maximum suggests a model weakness in the mixed layer while the RMSE maximum is related to a well-known feature of all ocean models due to uncertainty in the representation of the thermocline position.

The high vertical resolution of GOFS16 with respect to other systems (Ryan et al., 2015), combined with the assimilation of vertical profiles of in-situ data, seems to be beneficial for the best-estimate which shows a maximum error of 1°C at the thermocline depth. However, already at nowcast the error has increased by about 30%, suggesting that the model vertical mixing is not able to maintain an accurate initial state (Fig.10a). Both bias and errors tend to increase with increasing forecast lead days in the upper ocean but there are no significant differences at the following forecast days below their respective maximum depths. The results from the spatial maps (not shown) confirm that the regions of maximum errors in the upper ocean mirror those with the highest SST error, confirming the extratropical North Pacific region as a bad performing region

https://doi.org/10.5194/egusphere-2026-887
Preprint. Discussion started: 9 April 2026

in GOFS16. At the thermocline depths, large errors emerge all along the tropical band with values comparable to those in the mesoscale regions (not shown).

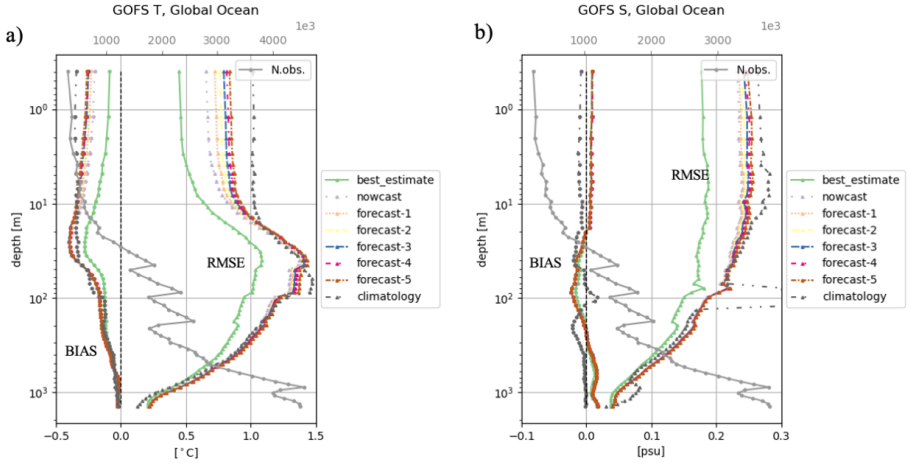

Figure10: a) Vertical temperature profiles for RMSE (solid lines) and bias (dotted lines) as function of the day of forecast and compared to the climatology averaged over 2022-2023. Gray line shows the number of observations. b) Same of a) but for salinity.

Figure 8b shows the same vertical analysis for the subsurface salinity. For this variable, we filter out observations with difference larger than 1 psu from climatology. This constrain ensures a meaningful comparison between model and climatology skill score, avoiding that spurious large values can saturate the final error. Differently from the temperature, the salinity bias is almost zero from the surface down to 1000m as the result of compensating biases of opposite signs. It shows a weak fresh bias emerging mainly in the Atlantic and Indian sectors of the ACC region, and a deeper and stronger salty bias characterizing most of the global ocean (from spatial maps, not shown). The salinity bias does not show any dependence on the forecast leading days, while the salinity RMSE increases by about 30% at nowcast with respect to the best estimate. This suggests that also the salinity initial state, although well constrained by the assimilation of vertical profiles, is not well maintained by the model mixing processes, which degrades both the temperature and salinity vertical representations in particular in the tropical band (not shown). However, in general both the salinity bias and errors in GOFS16 are well below the values of other global operation systems (Ryan et al., 2015; Liu et al., 2021) likely induced by a more accurate salinity assimilation. The spatial error patterns (not shown) show that the largest salinity errors in the upper ocean emerge in the Baltic Sea, the Black Sea, the Gulf Stream and Malvinas regions, and in correspondence of the Orinoco River mouth, suggesting possible issues with the climatological river runoff forcing (Dai and Trenberth, 2009) or with the discretization of runoff on the model grid.

The regional analysis of the depth-dependent RMSE of temperature and salinity of the nowcast indicates that the North Atlantic (orange line in Fig.11) is the region with the highest 1st day forecast errors over approximately the whole water column. Significantly large errors are evident also in the North Pacific and tropical Atlantic, at the thermocline depth for temperature and in the upper 100m for salinity. The South Pacific emerges as the region with the lowest errors around the thermocline and in salinity over the whole water column. However, this result needs to be better evaluated to exclude the possibility of being the effect of less abundant observations in this region since it seems to be a feature common to other systems (Ryan et al., 2015; Liu et al., 2021).

https://doi.org/10.5194/egusphere-2026-887
Preprint. Discussion started: 9 April 2026

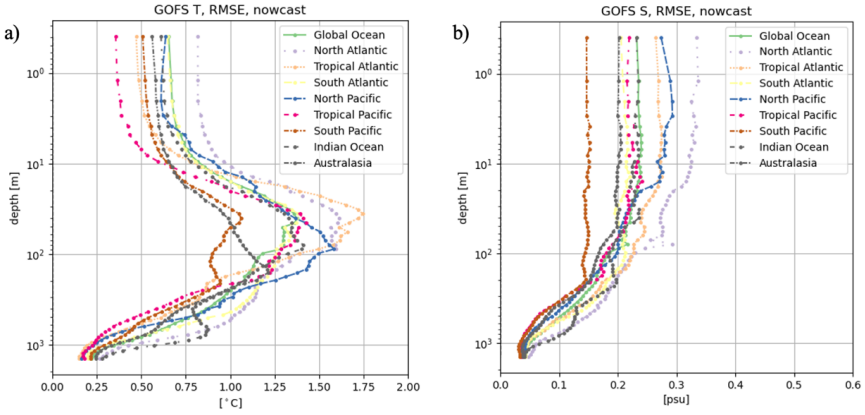

Figure 11: a) Vertical RMSE temperature profiles of the nowcast for different regions. b) Same of a) but for Salinity.

Several factors might contribute to the significant bias affecting in particular the subsurface temperature below 100m. We note here that the GOFS16 does not include any 3D damping for temperature and salinity, and the 24h assimilation window does not allow the inclusion of late-arrival observations which is usually more critical for subsurface observations less abundant than the surface ones. The initial condition in 2017 were derived from a 10-year free simulation of the ocean-ice configuration and one year of data assimilation (2016) without any bias correction, resulting in a subsurface ocean state which might still have biases due to unconstrained large-scales. The space and time resolution of the in-situ observations and the way in which the assimilation scheme spreads the corrections horizontally are also possible limiting factors, which prevent the forecast systems from providing skillful information across all spatial and temporal scales. The horizontal correlation length scales used in OceanVar is adequate to capture mesoscale features but are less effective to constrain the tracer fields at depth due to sparsity of sub-surface observations, suggesting the need to introduce a vertical dependence of the observation influence.

4.3 Global and regional surface currents

Surface currents are part of the Essential Climate Variables (ECV) since 2014 (Bojinski et al 2014) and became later part of the Essential Ocean Variables (EOV) thanks to the Ocean Observations Physics and Climate (OOPC) Panel. An accurate quantification of surface currents was acknowledged to be essential for understanding the ocean flow at different timescale, to predict the evolution of diverse climate indexes close to the coastlines, to design future off-shore renewable power plants or to forecast the movements of marine debris.

In literature, the standard approach to assess the quality of simulated currents is the direct comparison of the two components (zonal and meridional velocities) against estimates from drifters (Mignac et al., 2025; Lellouche et al., 2018). This assessment is presented here for GOFS16 as a function of the forecast lead day. However, it is worth to stress that model currents monitor dynamics that occur at different timescales with respect to drifter observations (Röhrs et al., 2021). The direct comparison is largely biased by the difference in time-averaging between model (daily) and observations (instantaneous), not to mention several phenomena that are not resolved by the model such as Stokes drift, tidal currents, near-inertial oscillation, etc. Moreover, OGCMs generally lack of correct coupling mechanisms for air-sea interactions under severe weather conditions (Renault et al., 2020). All these phenomena have a significant impact on local dynamics, limiting the inference from global forecasting information to specific regional prediction skills.

To enrich the discussion from a more scientific point of view, we compare GOFS16 currents against Ocean Surface Current Analyses Real-time (OSCAR) data that provide global estimate of daily surface ocean currents.

https://doi.org/10.5194/egusphere-2026-887
Preprint. Discussion started: 9 April 2026

4.3.1 Validation against OSCAR dataset

OSCAR fields are satellite-based currents that combine different contributions from geostrophic velocities, wind-driven effects and thermal wind adjustments (Bonjean and Lagerloef, 2002). Data are vertically averaged over a surface layer thickness of 30 m and interpolated on a 0.25° grid at daily frequency (ESR, 2022). Figure 12 shows the daily maps of GOFS16 ocean current best estimate against OSCAR, focusing on the biases and correlation for both zonal (U) and meridional (V) components over the period 2022-2023. The equatorial band is the zone with a persistent zonal bias that is positive over the eastern equatorial Pacific (about 0.2-0.3 m s^{-1}) and turns negative in the western equatorial Pacific with similar amplitude. The Indonesian area is also characterized by biases both in zonal and meridional components, although OSCAR quality degrades close to the coastlines. Significant biases are seen also at the mouth of the Amazon River and nearby areas.

Daily variability seems to be reasonably captured by GOFS16 best estimate, that shows a positive correlation with the daily OSCAR maps for both U and V almost everywhere, except in mesoscale-active region such as the Gulf Stream, Kuroshio and ACC where values are not significant (statistical significance over 2 years period is ~0.1). Zonal correlation is sensibly higher in the tropical region up to about 0.8.

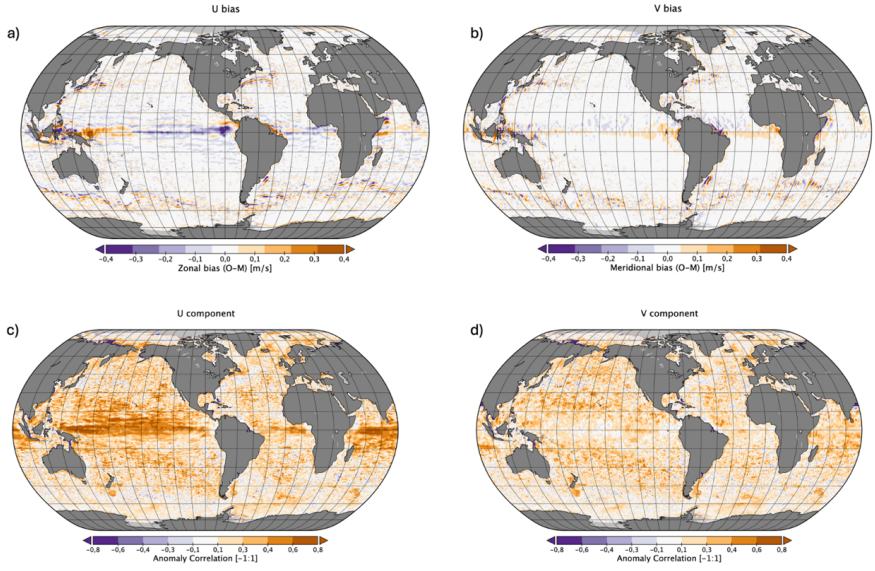

Fig.12: a) Map of the zonal velocity bias averaged over 2022-2023 (best estimate). b) Same as in a) but for the meridional velocity. c) Map of the zonal velocity anomaly correlation averaged over 2022-2023 (best estimate). d) Same as in c) but for the meridional velocity.

4.3.2 Validation against drifters

Drifters are part of the NOAA-funded Global Drifter Program (GDP), drogued at a nominal depth of 15m to minimize the wind- and wave-induced bias. Delayed-mode data are distributed with quality control, interpolated to regular 6-hour intervals (Lumpkin and Centurioni, 2019) by the Atlantic Oceanographic and Meteorological Laboratory (AOML, https://www.aoml.noaa.gov/phod/gdp/). Less than 5% of the data records are discarded due to unrealistic values or location errors (lon/lat measurement error that exceed the 0.01°). Another 1% is removed due to interpolation error. The analysis is

https://doi.org/10.5194/egusphere-2026-887
Preprint. Discussion started: 9 April 2026

divided in two different regions according to the mesoscale activity (high/low region) inferred by the standard deviation of the SLA (σ_{SLA}>0.11m/σ_{SLA}<=0.11m) (Blockley et al., 2014). The total number of observations considered is about ~2.5 million for "low" region and 0.5 million for the "high" region. Table 3 shows the evolution of the RMSE for the two horizontal components of the velocities with the day of forecast in the two regions. In the "low" region, the lowest RMSE is around 0.18 m/s for both the components while it raises up to 0.31 m/s in the "high" region and slowly increases with the forecast lead time.

Table 3: Model velocity RMSE against in-situ drifter velocities for best estimate, nowcast and forecasts. Statistics are divided in "low" (σ_{SLA}<=0.11 m) and "high" (σ_{SLA}>0.11 m) regions.

	BE	**Nowcast**	**FC (1st d)**	**FC(2nd d)**	**FC(3rd d)**	**FC(4th d)**	**FC(5th d)**
	RMSE [m/s]	RMSE [m s^{-1}]	RMSE [m s^{-1}]	RMSE [m s^{-1}]	RMSE [m s^{-1}]	RMSE [m s^{-1}]	RMSE [m s^{-1}]
σ_{SLA}<=0.11 m							
U	0.186	0.187	0.192	0.196	0.197	0.198	0.199
V	0.178	0.179	0.184	0.187	0.188	0.189	0.190
σ_{SLA}>0.11 m							
U	0.307	0.309	0.313	0.316	0.319	0.320	0.322
V	0.305	0.307	0.311	0.314	0.316	0.318	0.319

4.4 Case Study: tropical cyclone Larry

As an additional qualitative assessment of the system performance, we performed an analysis of a tropical cyclone which developed in the Atlantic Ocean in 2021.

It is well known since the 1960s (Leipper, 1967) that tropical cyclones (TCs) and hurricanes, while moving over the ocean, induce significant changes in the ocean thermal structure, with transfer of heat from the ocean to the atmosphere. The variations of the ocean surface and subsurface temperatures during these events are mainly driven by intense vertical mixing due to wind-induced vertical shear of the ocean currents (Jaimes and Shay, 2009) and by upwelling associated with the Ekman pumping (Huang et al., 2009).

Here we analyze the response of GOFS16 to the Larry passage in the Atlantic Ocean. Larry is one of the three major hurricanes that populated the 2021 Atlantic hurricane season (Brown, 2021), and since Dorian in 2019, it is the longest-lived Atlantic major hurricane. Formed close to Africa on 31 August, it moved toward the eastern tropical Atlantic undergoing a rapid intensification. Larry persisted in the Atlantic Ocean for almost two weeks before making landfall in Newfoundland and being absorbed, on 12 September, by another larger extratropical cyclone moving eastward in the Labrador Sea. It became a major Category 3 hurricane early on 4 September (at 15.2ºN and 42.7ºW) and stayed a category 3 tropical cyclone for several days with its peak intensity of 205 km/h.

A cold wake in the SST is the most outstanding feature of the upper ocean response to a TC. The formation of a cold ocean wake behind Larry is shown in Fig. 13, by the SST distribution in the North Atlantic sector on 10 September when Larry was located at 38.9ºN and 61ºW. The broad-scale SST cooling is visible following the hurricane track and is placed on the right-side of its path (Zhang et al., 2021). The cooling (up to ~3ºC compared to environmental water) appears shortly after Larry passage and takes several days to recover.

https://doi.org/10.5194/egusphere-2026-887
Preprint. Discussion started: 9 April 2026

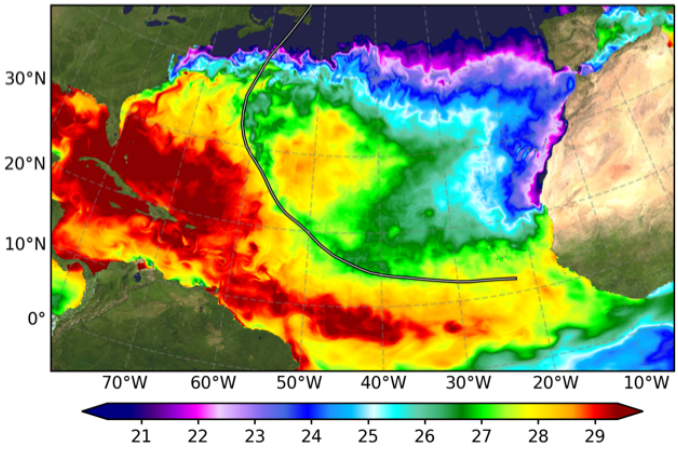

Figure13: Daily mean SST (in ºC) on 10 September 2021, with Larry track position (31 August – 11 September) based on NOAA National Hurricane Center data (https://www.nhc.noaa.gov/).

The characteristics of the upper-ocean thermal response to a TC are affected by cyclones intensity, size and translation speed (e.g. Lin et al., 2017). For relatively-weak TCs (≤ Category 3), the subsurface water tends to cool with air–sea heat exchange and upwelling prevailing on mixing and downwelling that in turn tend to generate subsurface warm anomalies (Zhang et al., 2021). Fig. 14 presents the pre-hurricane conditions and the evolution of temperature in the upper 110 m of the ocean column at 12 p.m. UTC of each day from three locations (between 20ºN and 30ºN) for the entire life span of Larry. GOFS16 captures hurricane-forced changes with the upper-ocean thermal structure disrupted over each Larry position. The daily means of the GOFS16 temperature profiles show severe upwelling of cold thermocline water of less than ~25°C during and after Larry passes over the specific location. Water masses deeper than ~100m rise towards the sea surface with temperature lower than the pre-hurricane conditions.

The magnitude and the duration of cooling vary depending on the hurricane characteristics and pre-existing upper-ocean conditions such as the presence of ocean mesoscale eddies and upper-ocean stratification. Within the upper 20m, the ocean temperature decreases by less than 1°C and the change lasts only a day in the southernmost location, while it decreases by up to 3°C and recovers to pre-Larry conditions in almost a week, in the other two locations.

Changes in the ocean temperature are linked to the density (and hence salinity) structures, as stratification can inhibit vertical mixing even under hurricane winds (e.g. Vincent et al., 2012). Moreover, surface freshwater fluxes, in addition to vertical mixing and upwelling in the ocean, are affected by intense rainfall and evaporation associated to TC winds (Sun et al., 2021). The combined effect of Larry on the subsurface thermal and salinity structures and consequent impact on density is presented through TS diagrams for the upper 100 m, before and after the passage of the hurricane in the same three locations (Fig.14, bottom panels). The salinity response to Larry depends on depth and changes with the locations. GOFS16 shows upper-layer densification from pre- to post-hurricane conditions. In the surface layer at 21.6°N, there is a salinification that, together with cooling, results in increased density, while salinity slightly reduces going deeper. At 24°N, the salinity changes are reversed with freshening of the surface waters and deeper salinification. At 27.2°N, a salinity reduction is reproduced soon after Larry passage throughout the 100m layer and freshening persists till 15 September. The differences among these 3 locations are likely linked to the pre-hurricane conditions, but also to the eventual presence of eddies in the regions (e.g. Yablonsky and Ginis, 2012; Liu et al., 2021).

https://doi.org/10.5194/egusphere-2026-887
Preprint. Discussion started: 9 April 2026

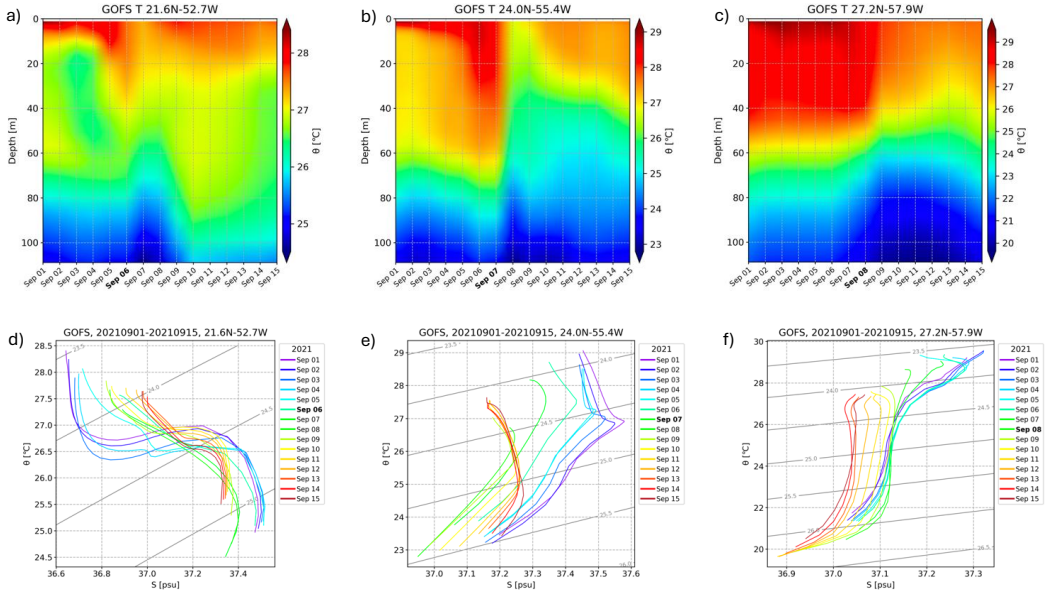

Figure14: a-c) Hovmöller diagrams of the upper-ocean potential temperature between 1 and 15 September (at 12pm UTC) at three selected positions along Larry track. The bold date on the x-axis indicates which day Larry passes at that location. d- f): Potential temperature-salinity (TS) diagrams of GOFS16 best estimate in the upper 100m over the same period and locations, with isopycnals superimposed.

5. Summary, discussion, and future developments

The Global Ocean Forecast System GOFS16 is an operational ocean analysis and forecast system at 1/16° horizontal resolution that runs daily at the Euro-Mediterranean Center on Climate Change since early 2017. The system is based on a global eddying ocean configuration combined with a state-of-the-art variational data assimilation system that is capable of assimilating both space-borne and conventional observing networks, including hydrographic profiles and multiple satellite data, at the same resolution of the model. In this work, we present the main components of the systems and provide a preliminary assessment of GOFS16 forecast skills by means of conventional error and bias analyses. Each analysis and forecast produced by GOFS16 addresses two key problems: what is the best estimate of the current state of the ocean based on observations and how to forecast processes at the meso-scale. Despite the growing number of freely accessible observations year by year, the system is still largely unconstrained, i.e. the number of independent data available is much less than the dimension of ocean state.

Since January 2021, GOFS16 has joined the OceanPredict inter-comparison project that gathers and compares different global prediction systems at different resolutions. Routine evaluation of the current system skills, accompanied by bug fixing and continuous improvements since its implementation, has been encouraging and confirms the capacity of GOFS16 to perform within the range of the other global systems.

There are several factors potentially responsible for the limited improvements in the forecast skills brought by increased model resolution (e.g. Barbosa Aguiar, 2024). The computational resources have allowed the ocean modelling resolution to grow significantly in the last decade allowing to go from eddy-permitting to eddy-resolving capability. However, ocean observation coverage has not expanded at the same level and this situation is leading to an apparent degraded forecast skill when model resolution is increased but the same forcing fields and assimilating the same set of observations are used

https://doi.org/10.5194/egusphere-2026-887
Preprint. Discussion started: 9 April 2026

(Hernandez et al., 2015; Barbosa Aguiar et al., 2021). This behaviour reflects the so-called double-penalty effect, which occurs in typical verification metrics such as the RMSE and penalizes the high-resolution systems. The double-penalty effect appears when features are correctly forecasted but displaced with respect to the observation, thus being counted twice as errors: once because they are not occurring at the forecast location and again because they occur at a location where they have not been observed (Crocker et al., 2020).

In synthesis, it should be noted that the traditional Class 4 metrics might not be adequately to capture the predictive capability of eddy-rich systems, such as GOFS16. Alternative verification methods, the so-called "spatial" verification methods widely used in the atmospheric community, have been suggested to account for the fact that realistic mesoscale features may not be forecasted at the exact observed place and time. Neighbourhood verification methods (Crocker et al., 2020), which use common spatial scales for comparison between configurations of different resolutions (Barbosa Aguiar et al., 2021), and spectral analysis of the forecast error (Thoppil et al., 2021), which mitigates the double-penalty effect at scales not contaminated by observational noise, should be considered in the future for the assessment of mesoscale resolving systems. Also, the observations used for the Class 4 metrics might contribute to the penalty effect since they are not able to reliably assess the eddy-capability of the systems. For example, SLA assessment could be performed using along-track satellite observations filtered differently, to capture more mesoscale features. Similarly, model SST could be compared with the highest resolution and most reliable SST products provided in near-real time (Hernandez et al., 2015). A similar issue might occur when we compare eddy-resolving systems against climatological fields with much coarser horizontal and vertical resolution. In the GOFS16 case, for example, the resolution of the climatology is four times coarser than the forecast system resolution.

The initial conditions in eddy-resolving forecasting systems are difficult to constrain with the present number and distribution of observations. High uncertainty in the initial location and evolution of mesoscale features limits the spatial scales at which ocean forecast system can provide skillful information. Although eddy-resolving models often reproduce energy and mesoscale features of realistic size and magnitude (Chassignet et al., 2020; Iovino et al., 2023), their positions are typically not accurate. The initial conditions are still mainly constrained by satellite altimeters and SST, while the subsurface ocean suffers from the sparse availability of in situ data and the errors introduced by data assimilation techniques when projecting surface information into the ocean interior. It has been shown that ensemble forecasting methods, which account for this uncertainty and filter the unconstrained scales, can significantly reduce errors in both the analysis and forecast (Thoppil et al., 2021). In this context, the term constrained indicates features in a forecast system for which there are sufficient observations to provide a skillful forecast, and vice-versa for unconstrained (Jacobs et al., 2019). More rigorously, constrained scales are those for which the power spectral density (PSD) of the errors is smaller than the PSD of the true fields, and it has been shown to be approximately 160 km when the SSH is considered (D'Addezio et al., 2019). Using 1000 independent surface drifters and Observations System Simulation Experiment (OSSE), Jacobs et al. (2021) show that constrained scales have deterministic prediction skill and unconstrained scales are affected by higher errors. Results from an ensemble experiment showed energy reduction at unconstrained scales, suggesting uncorrelated features among the ensemble members at the smaller scales. This helps to explain why increasing resolution often is accompanied by increased variance at unconstrained scales, leading to degraded forecast skills (Sandery and Sakov, 2017).

One way to reduce the uncertainties is to increase the density of the ocean sampling networks. For example, the Surface Water/Ocean Topography (SWOT) satellite mission will provide dense but still patchy observations daily. Underwater gliders and denser drifter deployments will provide dense observations but mainly useful for targeted regions. The other way might be offered by coarser resolution ensemble forecasting methods which should complement the current effort on higher-resolution forecasting system.

The on-going developments of GOFS16 include an updated version of both the ocean and sea-ice models and the use of atmospheric forcing at higher resolution and higher frequency, which could contribute to the reduction of the large error

https://doi.org/10.5194/egusphere-2026-887
Preprint. Discussion started: 9 April 2026

increase of the current version of the system from the best estimate to next forecast day. In terms of assimilation, we are working on the modification of the operational chain to allow for a once-a-week assimilation of a larger number and better-quality observations.

In the future, we aim to analyse the impact of correlation length scales to evaluate the observations influence in the surrounding areas. Formally, this scale represents the spatial correlation of errors in the model initial conditions, and its size could influence the constrained scales. In addition, we propose to start investigating multi-scale analysis technique (Li et al., 2015; Chamberlain et al., 2021) in which two assimilation steps correct the ocean at separate length scales: the first step is meant to correct scales resolved by coarse observations and the second step the smaller scales resolved by patchy dense data. The continuous intercomparison of GOFS16 with other more mature but coarser resolution global forecasting systems and the introduction of verification skill scores using more advanced methods (e.g., Crocker et al., 2020 and Thoppil et al., 2021) will help to identify its main weaknesses and inspire possible future refinements/developments to further improve its quality.

Data availability

GOFS16 model equivalents can be found in https://doi.org/10.5281/zenodo.18504242 (Cipollone, 2026). Full datasets of temperature, salinity, sea level anomaly and sea surface temperature are available within GODAE/OceanPredict intercomparison project from the ECCC external computing cluster. Estimates of zonal and meridional components of ocean currents from NOAA Global Drifter Programs are available from https://www.aoml.noaa.gov/phod/gdp/. Full model currents from the best estimate, are available by contacting directly the Authors due to the need of large storage. Model configuration is described and available at Iovino et al. 2016. Data assimilation configuration is described at Cipollone et al. 2020.

Author contributions

SM conceptualized the whole system and wrote the manuscript. AC and DI developed the data assimilation and model configuration steps respectively and contribute to the writing. SC and SC developed the operational chain and review the manuscript. RL modified and monitored the chain operationally and contributes to the writing. VL developed the website for validation and reviewed the manuscript. GC and EC supervised the system and review the manuscript.

Competing interests

The authors declare that they have no conflict of interest.

References

Arakawa, A. and Lamb, V. R.: "A potential enstrophy and energy conserving scheme for the shallow water equations", Mon. Weather Rev., 109, 18-36, doi: 10.1175/1520-0493(1981)109<0018:APEAEC>2.0.CO;2 ,1980.

Axell, L. B.: "Wind-driven internal waves and Langmuir circulations in a numerical ocean model of the southern Baltic Sea", J. Geophys. Res., 107, 3204, doi:10.1029/2001JC000922, 2002.

Barbosa Aguiar, A., Waters, J , Price M., Inverarity G., Pequignet, C. et al.: "The new met office global ocean forecast system at 1/12° resolution",. 9thEuroGOOS International conference, Shom; Ifremer; EuroGOOS AISBL, , Brest, France, 2021

Barbosa Aguiar, A., Bell, M.J., Blockley, E., Calvert, D., Crocker, R., Inverarity, G. et al. :"The Met Office Forecast Ocean Assimilation Model (FOAM) using a 1/12-degree grid for global forecasts", Quarterly Journal of the Royal Meteorological Society, 1–26. https://doi.org/10.1002/qj.4798 , 2024.

Barnier, B., Madec, G., Penduff, T., Molines, J. M., Treguier, A. M., Le Sommer, J., Beckmann, A., Biastoch, A., Boning, C., Dengg, J., Derval, C., Durand, E., Gulev, S., Remy, E., Talandier, C., Theetten, S., Maltrud, M., McClean, J., and De

https://doi.org/10.5194/egusphere-2026-887
Preprint. Discussion started: 9 April 2026

Cuevas, B.: "Impact of partial steps and momentum advection schemes in a global ocean circulation model at eddy permitting resolution", Ocean Dynam., 56, 543-567, doi: 10.1007/s10236-006-0082-1, 2006.

Bellucci, A., S. Masina, P. Di Pietro, and A. Navarra: "Using temperature salinity relations in a global ocean implementation of a multivariate data assimilation scheme", Mon. Wea. Rev., 135, 3785–3807 , doi: 10.1175/2007MWR1821.1, 2007.

Bernie, D., Guilyardi, E., Madec, G., Slingo, J. M., and Woolnough, S. J.: "Impact of resolving the diurnal cycle in an ocean-atmosphere GCM. Part 1: a diurnally forced OGCM", Clim. Dynam., 29, 575-590, doi: 10.1007/s00382-007-0249-6, 2007.

Blanke, B. and Delecluse, P.: "Variability of the tropical Atlantic Ocean simulated by a general circulation model with two different mixed-layer physics", J. Phys. Oceanogr., 23, 1363-1388, doi: 10.1175/1520-0485(1993)023<1363:VOTTAO>2.0.CO;2 , 1993.

Blockley EW, Martin MJ, McLaren AJ, Ryan AG, Waters J, Lea DJ, Mirouze I, Peterson KA, Sellar A, Storkey D. : "Recent development of the Met Office operational ocean fore- casting system: an overview and assessment of the new Global FOAM forecasts", Geosci Model Dev. 7: 2613–2638, doi:10.5194/gmd-7-2613-2014, 2014.

Bojinski, S., M. Verstraete, T. C. Peterson, C. Richter, A. Simmons, and Zemp M.,: "The Concept of Essential Climate Variables in Support of Climate Research, Applications, and Policy", *Bull. Amer. Meteor. Soc., 95,* 1431–1443, doi: 10.1175/BAMS-D-13-00047.1 , 2014.

Bonjean, F., and G. S. E. Lagerloef: "Diagnostic Model and Analysis of the Surface Currents in the Tropical Pacific Ocean", J. Phys. Oceanogr., 32, 2938–2954, doi: 10.1175/1520-0485(2002)032<2938:DMAAOT>2.0.CO;2 , 2002.

Bourdalle-Badie, R., and Treguier, A. M.: "A climatology of runoff for the global ocean-ice model ORCA025", Report, Mercator-Ocean. Reference: MOO-RP-425-365-MER, 2006.

Bouillon, S., Morales Maqueda, M. A., Legat, V., and Fichefet, T.: "An elastic-viscous-plastic sea ice model formulated on Arakawa B and C grids", Ocean Model., 27, 174-184, doi: 10.1016/j.ocemod.2009.01.004 , 2009.

Boyer, T., Levitus, S., Garcia, H., Locarnini, R. A., Stephens, C., & Antonov, J.,"Objective analyses of annual, seasonal, and monthly temperature and salinity for the World Ocean on a 0.25 grid", International Journal of Climatology: A Journal of the Royal Meteorological Society, 25(7), 931-945, doi: 10.1002/joc.1173 , 2005.

Brassington, G.B., Freeman, J., Huang, X., Pugh, T., Oke, P.R., Sandery, P.A., Taylor, A., Andreu-Burillo, I., Schiller, A., Griffin, D.A., Fiedler, R., Mansbridge, J., Beggs, H., Spillman, C.M. :"Ocean Model Analysis and Prediction System: Version 2", CAWCR Technical Report (052), The Centre for Weather and Climate Research, 2012.

Broccoli, M. and Cipollone A. :"Assimilation of diurnal satellite retrieval of sea surface temperature with convolutional neural network", Mach. Learn.: Earth 1, 015007, doi: 10.1088/3049-4753/adfb7e , 2025.

Brown, D.:" Tropical Cyclone Report: Hurricane Larry " ,Report, Miami, Florida: National Hurricane Center,2021.

Chamberlain M.A., P.R. Oke, G.B. Brassington, P. Sandery, P. Divakaran, R.A.S. Fiedler: "Multiscale data assimilation in the Bluelink ocean reanalysis (BRAN)", Ocean Modelling, Volume 166, doi: 10.1016/j.ocemod.2021.101849, 2021.

Chassignet, E. P., Yeager, S. G., Fox-Kemper, B., Bozec, A., Castruccio, F., Danabasoglu, G., Horvat, C., Kim, W. M., Koldunov, N., Li, Y., Lin, P., Liu, H., Sein, D. V., Sidorenko, D., Wang, Q., and Xu, X.: "Impact of horizontal resolution on global ocean–sea ice model simulations based on the experimental protocols of the Ocean Model Intercomparison Project phase 2 (OMIP-2)", Geosci. Model Dev., 13, 4595–4637,doi : 10.5194/gmd-13-4595-2020 , 2020.

Ciliberti, S.A., Jansen, E., Coppini, G., Peneva, E., Azevedo, D., Causio, S., Stefanizzi, L., Creti', S.,Lecci, R., Lima, L., et al. : "The Black Sea Physics Analysis and Forecasting System within the Framework of the Copernicus Marine Service", J. Mar. Sci. Eng., 10, 48, doi: 10.3390/jmse10010048 , 2022.

Cipollone, A., Storto, A., and Masina, S.: "Implementing a parallel version of a variational scheme in a global assimilation system at eddy-resolving resolution", Journal of Atmospheric and Oceanic Technology, *37*(10), 1865-1876, doi: 10.1175/JTECH-D-19-0099.1, 2020.

https://doi.org/10.5194/egusphere-2026-887
Preprint. Discussion started: 9 April 2026

Cipollone, "Model equivalents from a global ocean forecasting system at eddy-resolving resolution", zenodo, https://doi.org/10.5281/zenodo.18504242, 2026

Cooper, M., and K. Haines: "Altimetric assimilation with water property conservation", J. Geophys. Res., 101, 1059–1077 , doi: 10.1029/95JC02902,1996

Coppini, G., Clementi, E., Cossarini, G., Salon, S., Korres, G., Ravdas, M., et al. .: "The Mediterranean Forecasting System–Part 1: Evolution and performance", Ocean Science, 19(5), 1483-1516, doi: 10.5194/os-19-1483-2023 , 2023.

Courtier, P., 1997: "Variational methods", J. Meteorol. Soc. Japan, 75, 211–218, 1997

Crocker, R., Maksymczuk, J., Mittermaier, M., Tonani, M., and Pequignet, C. : "An approach to the verification of high-resolution ocean models using spatial methods", Ocean Science, 16(4), 831-845, doi: 10.5194/os-16-831-2020, 2020.

D'Addezio, J.M., Smith, S., Jacobs, G.A., Helber, R.W., Rowley, C., Souopgui, I., Carrier, M.J. : "Quantifying wavelengths constrained by simulated SWOT observations in a submesoscale resolving oceananalysis/forecasting system", Ocean Model. 135, 40–55, doi: 10.1016/j.ocemod.2019.02.001,2019.

Dai, A., Qian, T., Trenberth, K. E., and Milliman, J. D.: "Changes in continental freshwater discharge from 1948-2004", J. Climate, 22, 2773-2791, doi: 10.1175/2008JCLI2592.1, 2009.

Davidson, F., Alvera-Azcarate, A., Barth, A., Brassington, G. B., Chassignet, E. P., Clementi, E., et al. : "Synergies in operational oceanography: the intrinsic need for sustained ocean observations", Frontiers in Marine Science, *6*, 450, doi: 10.3389/fmars.2019.00450, 2019.

De Dominicis, M., Leuzzi, G., Monti, P., Pinardi, N., and Poulain, P. M.: "On the development of a coastal ocean forecasting system for the Adriatic Sea", Ocean Science, 10, 673–690, doi: 10.5194/os-10-673-2014, 2014

Dobricic, S., and N. Pinardi: "An oceanographic three-dimensional variational data assimilation scheme", Ocean Modelling, 22, 89-105, doi: 10.1016/j.ocemod.2008.01.004 , 2008.

Ebert, E., Wilson, L., Weigel, A., Mittermaier, M., Nurmi, P., Gill, P., Göber, M., Joslyn, S., Brown, B., Fowler, T. and Watkins, A.: "Progress and challenges in forecast verification", Met. Apps, 20: 130-139, doi: 10.1002/met.1392 , 2013.

EMODnet, temperature and salinity data are available from EMODnet physics portal (https://portal.emodnet-physics.eu) that is owned by the EU and licensed under the Creative Commons Attribution 4.0 International (CC BY 4.0) license. Last access : 23-01-2026, 2026

ESR; Dohan, Kathleen. Ocean Surface Current Analyses Real-time (OSCAR) Surface Currents - Final 0.25 Degree (Version 2.0). Ver. 2.0. PO.DAAC, CA, USA. Last access : 23-01-2026, doi: 10.5067/OSCAR-25F20 , 2022

EUMETSAT/OSI SAF, GHRSST L3C global SST from AVHRR on Metop-B produced by OSI SAF. Ver. 1. PO.DAAC, CA, USA. Last access: 23-01-2026, doi: 10.5067/GHGMB-3CO02, 2016

Fichefet, T. and Morales Maqueda, M. A.: "Sensitivity of a global sea ice model to the treatment of ice thermodynamics and dynamics", J. Geophys. Res., 102, 12609-12646, doi: 10.1029/97JC00480 ,1997.

Fox-Kemper, B., Adcroft, A., Böning, C. W., Chassignet, E. P., Curchitser, E., Danabasoglu, G., ... & Yeager, S. G. : "Challenges and prospects in ocean circulation models", Frontiers in Marine Science, 6, 65, doi: 10.3389/fmars.2019.00065 ,2019

Fretwell, P., Pritchard, H. D., Vaughan, D. G., Bamber, J. L., Barrand, N. E., Bell, R., Bianchi, C., Bingham, R. G., Blankenship, D. D., Casassa, G., Catania, G., Callens, D., Conway, H., Cook, A. J., Corr, H. F. J., Damaske, D., Damm, V., Ferraccioli, F., Forsberg, R., Fujita, S., Gim, Y., Gogineni, P., Griggs, J. A., et al.: "Bedmap2: improved ice bed, surface and thickness datasets for Antarctica", The Cryosphere, 7, 375-393, doi:10.5194/tc-7-375-2013, 2013.

Garraffo, Z.D., J.A. Cummings, S. Paturi, Y. Hao, D. Iredell, T. Spindler, B. Balasubramanian, I. Rivin, H-C. Kim, A. Mehra: "RTOFS-DA: Real Time Ocean-Sea Ice Coupled Three Dimensional Variational Global Data Assimilative Ocean Forecast System", Research Activities in Earth System Modelling, edited by E. Astakhova, WMO, World Climate Research Program Report No.6, 2020

https://doi.org/10.5194/egusphere-2026-887
Preprint. Discussion started: 9 April 2026

GDPFS WMO, Global Data-processing and Forecasting System of the WMO, 485 Vol. I , 2010Good S. A., Martin M. J. and Rayner N. A. : "EN4: quality controlled ocean temperature and salinity profiles and monthly objective analyses with uncertainty estimates*"* ,J. Geophys. Res. Oceans 118 6704–16, doi: 10.1002/2013JC009067, Last Access 23-01-2026, 2013.

Hallberg, R.: "Using a resolution function to regulate parameterizations of oceanic mesoscale eddy effects", Ocean Modelling, *72*, 92-103,doi: 10.1016/j.ocemod.2013.08.007, 2013

Hernandez F, Bertino L, Brassington GB, Chassignet E, Cummings j, Davidson F, Drévillon M, Garric G, Kamachi M, Lellouche J-M, et al.: "Validation and intercom-parison studies within GODAE", Oceanogr. 22 (3):128–143, 2009

Hernandez F, Blockley E, Brassington GB, Davidson F, Divakaran P, Drévillon M, Ishizaki S, Garcia-Sotillo M, Hogan PJ, Lagemaa P, Levier B. : "Recent progress in performance evaluations and near real-time assessment of operational ocean products", J. Oper. Oceanogr. 8(sup2): s221–s238, doi: 10.1080/1755876X.2015.1050282 , 2015

Hoffman, R. N., Z. Liu, J. Louis, and C. Grassoti: "Distortion Representation of Forecast Errors.", Mon. Wea. Rev., 123, 2758–2770, doi: 10.1175/1520-0493(1995)123<2758:DROFE>2.0.CO;2 ,1995.

Huang, B.; Liu, C.; Banzon, V. F.; Freeman, E.; Graham, G.; Hankins, W.; Smith, T. M.; Zhang, H.-M. :"NOAA 0.25-degree Daily Optimum Interpolation Sea Surface Temperature (OISST), Version 2.1", NOAA National Centers for Environmental Information, doi: 10.25921/RE9P-PT57, Last access : 23-01-2026, 2020

Huang P. S., Sanford T.B., Imberger J.:"Heat and turbulent kinetic energy budgets for surface layer cooling induced by the passage of Hurricane Frances (2004)", Journal of Geophysical Research 114: C12023,doi: 10.1029/2009JC005603 ,2009.

Hunke, E. C. and Dukowicz, J. K.: "An elastic-viscous-plastic model for sea ice dynamics", J. Phys. Oceanogr., 27, 1849-1867, doi: 10.1175/1520-0485(1997)027<1849:AEVPMF>2.0.CO;2 ,1997.

INSITU_GLO_PHYBGCWAV_DISCRETE_MYNRT_013_030. E.U. Copernicus Marine Service Information (CMEMS). Marine Data Store (MDS). doi: 10.48670/moi-00036 , Last Access: 23-01-2026, 2026.

IOC, IHO and BODC: "Centenary Edition of the GEBCO Digital Atlas", published on behalf of the Intergovernmental Oceanographic Commission and the International Hydrographic Organization as part of the General Bathymetric Chart of the Oceans, British Oceanographic Data Centre, Liverpool, UK, 2003.

Iovino, D., Masina, S., Storto, A., Cipollone, A., and Stepanov, V. N.: "A 1/16 eddying simulation of the global NEMO sea ice-ocean system", Geosci. Model Dev., 9, 2665-2684, doi: 10.5194/gmd-9-2665-2016, 2016.

Iovino, D., Fogli, P. G., and Masina, S. : "Evaluation of the CMCC global eddying ocean model for the Ocean Model Intercomparison Project (OMIP2)", Geoscientific Model Development, 16(21), 6127-6159, doi: 10.5194/gmd-16-6127-2023, 2023

Jacobs G.A., J. M. D'Addezio, B. Bartels et al.: "Constrained scales in ocean forecasting", Advances in Space Research, doi: 10.1016/j.asr.2019.09.018 ,2019.

Jacobs G., J.M. D'Addezio, H. Ngodock, I.Souopgui: "Observation and model resolution implications to ocean prediction", Ocean Modelling, Volume 159, doi: 10.1016/j.ocemod.2021.101760, 2021.

Jaimes B., Shay L. K. :"Mixed layer cooling in mesoscale oceanic eddies during hurricanes Katrina and Rita". Monthly Weather Review 137: 4188-4207, doi: 10.1175/2009MWR2849.1 , 2009

Large, W. and Yeager, S.: "Diurnal to decadal global forcing for ocean sea ice models: the data set and fluxes climatologies", Rep. NCAR/TN-460CSTR, National Center for Atmospheric Research, Boulder, Colorado, USA, 2004.

Leipper, D. F.: "Observed Ocean Conditions and Hurricane Hilda, 1964", J. Atmos. Sci., 24, 182–186, doi: 10.1175/1520-0469(1967)024<0182:OOCAHH>2.0.CO;2 , 1967.

Lellouche J-M, Greiner E, Le Galloudec O, Garric G, Regnier C. : "Recent updates to the Copernicus Marine Service global ocean monitoring and forecasting real-time 1⁄12° high-resolution system", Ocean Sci. 14:1093–1126. doi:10.5194/os-14-1093-2018, 2018.

https://doi.org/10.5194/egusphere-2026-887
Preprint. Discussion started: 9 April 2026

Le Traon, P.-Y., Dibarboure, G., Jacobs, G., Martin, M., ReÅLmy, E., Schiller, A., :"Use of satellite altimetry for operational oceanography", Satellite Altimetry Over Oceans and Land Surfaces. CRC Press, Boca Raton, pp. 581–608, 2017.

Li, Z., McWilliams, J.C., Ide, K., Farrara, J.D., :"A multiscale variational data assimilation scheme: formulation and illustration", Mon. Weather Rev. 143 (9), 3804–3822, doi: 10.1175/MWR-D-14-00384.1, 2015

Lin, S., Zhang, W.-Z., Shang, S.-P., Hong. H.-S/ :"Ocean response to typhoons in the western North Pacific: composite results from Argo data", Deep-Sea Res, Part I 123:62–74, doi: 10.1016/j.dsr.2017.03.007, 2017

Liu, Y., Lu, H., Zhang, H., Cui, Y., Xing, X.: "Effects of ocean eddies on the tropical storm Roanu intensity in the Bay of Bengal", PLoS One. 2021 Mar 5;16(3):e0247521. doi: 10.1371/journal.pone.0247521, 2021.

Liu, H., Lin,P., Zheng W., Luan, Y., Ma J., Ding, M., Mo, H., Wan L. and Ling, T.: "A global eddy-resolving ocean forecast system in China – LICOM Forecast System (LFS)", Journal of Operational Oceanography, doi: 10.1080/1755876X.2021.1902680 , 2021.

Lumpkin, R. and Centurioni, L. :"Global Drifter Program quality-controlled 6-hour interpolated data from ocean surface drifting buoys", Dataset, last access: 23-01-2026, doi: 10.25921/7ntx-z961 , 2019

Madec, G., Benshila, R., Bricaud, C., Coward, A., Dobricic, S., Furner, R., and Oddo, P..: "NEMO ocean engine", Notes du Pôle de modélisation de l'Institut Pierre-Simon Laplace (IPSL) (v3.4, Number 27). Zenodo, doi: 10.5281/zenodo.1464817 , 2013.

Mellor, G. and Blumberg, A.: "Wave breaking and ocean surface layer thermal response", J. Phys. Oceanogr., 34 (3), 693-698, doi: 10.1175/2517.1 , 2004.

Mignac, D., Waters, J., Lea, D. J., Martin, M. J., While, J., Weaver, A. T., Vidard, A., Guiavarc'h, C., Storkey, D., Ford, D., Blockley, E. W., Baker, J., Haines, K., Price, M. R., Bell, M. J., and Renshaw, R. :"Improvements to the Met Office's global ocean–sea ice forecasting system including model and data assimilation changes", Geosci. Model Dev., 18, 3405–3425, doi: 10.5194/gmd-18-3405-2025 , 2025.

Murphy, A.H."What is a good forecast? An essay on the nature of goodness in weather forecasting", Weather Forecast. 8, 281–293, doi: 10.1175/1520-0434(1993)008<0281:WIAGFA>2.0.CO;2 , 1993.

NCEP GFS 0.25 Degree Global Forecast Grids Historical Archive. Research Data Archive at the National Center for Atmospheric Research, Computational and Information Systems Laboratory, Last Access: 28/01/2026, doi: 10.5065/D65D8PWK , , available online at https://rda.ucar.edu/datasets/ds084.1/ , 2026.

Prather, M.: "Numerical advection by conservation of second-order moments", Journal of Geophysical Research 91, 6671–6681, doi: 10.1029/JD091iD06p06671 ,1986.

Renault, L., Masson, S., Arsouze, T., Madec, G., & McWilliams, J. C. :"Recipes for how to force oceanic model dynamics", Journal of Advances in Modeling Earth Systems, 12, e2019MS001715, doi: 10.1029/2019MS001715 ,2020.

Remote Sensing Systems :"GHRSST Level 3U Global Subskin SST from the AMSR2. Ver. 8a", PO.DAAC, CA, USA, doi: 10.5067/GHAM2-3UR8A, last access 12-01-2026 , 2017.

Reynolds, R. W., Smith T.M., Liu C., Chelton D.B., Casey K.S. and Schlax M.G. :"Daily high-resolution blended analyses for sea surface temperature", J. Climate, 20, 5473–5496, doi: 10.1175/2007JCLI1824.1 ,2007.

Ryan, A.G., Regnier, C., Divakaran, P., Spindler, T., Mehra, A., Smith, G.C., Davidson, F., Hernandez, F., Maksymczuk, J., Liu, Y. : "GODAE oceanview class 4 forecast verification fra- mework: global ocean inter-comparison", J. Oper. Oceanogr. 8(sup1): s98–s111, doi: 10.1080/1755876X.2015.1022330 , 2015.

Röhrs, J., Sutherland, G., Jeans, G., Bedington, M., Sperrevik, A. K., Dagestad, K. F. and LaCasce, J. H. "Surface currents in operational oceanography: Key applications, mechanisms, and methods", Journal of Operational Oceanography, 16(1), 60–88, doi: 10.1080/1755876X.2021.1903221,, 2021

Roullet, G. and Madec, G.: "Salt conservation, free surface and varying levels: a new formulation for ocean general circulation models", J. Geophys. Res., 105, 23927-23942, doi: 10.1029/2000JC900089 , 2000.

https://doi.org/10.5194/egusphere-2026-887
Preprint. Discussion started: 9 April 2026

SEALEVEL_GLO_PHY_L3_NRT_008_044. E.U. Copernicus Marine Service Information (CMEMS). Marine Data Store (MDS). doi: 10.48670/moi-00147 , Last Access : 23-01-2026, 2026

SEALEVEL_GLO_PHY_L4_NRT_008_046. E.U. Copernicus Marine Service Information (CMEMS). Marine Data Store (MDS). doi: 10.48670/moi-00149 , Last Access: 23-01-2026, 2026

Schiller, A., Bell, M., Brassington, G., Brasseur, P., Barciela, R., De Mey, P., et al. : "Synthesis of new scientific challenges for GODAE OceanView", Journal of Operational Oceanography, 8(sup2), s259-s271, doi: 10.1080/1755876X.2015.1049901, 2015

Schiller, A., Baptiste, M., Yann, D., and Gary, B.: "An overview of operational oceanography," New Frontiers in Operational Oceanography, eds E. Chassignet, A. Pascual, J. Tintoré, and J. Verron (France: GODAE OceanView), 1–26. doi: 10.17125/gov2018.ch01, 2018

Shine, K.P., Henderson-Sellers, A. :"The sensitivity of a thermodynamic sea ice model to changes in surface albedo parameterization" ,Journal of Geophysical Research 90, 2243–2250, doi: 10.1029/JD090iD01p02243 ,1985

Sloyan, B.M., M. Roughan, and K. Hill: "The global ocean observing system", New Frontiers in Operational Oceanography, E. Chassignet, A. Pascual, J. Tintoré, and J. Verron, Eds., GODAE OceanView, 75-90, doi: 10.17125/gov2018.ch03, 2018

Smith, N., and Lefebvre, M. :"The global ocean data assimilation experiment (GODAE)," ,Paper presented at Monitoring the Oceans in the 2000s, Vol. 1, (France), 1997. doi: 10.1016/j.marpolbul.2011.06.026 , 1997

Smith, G. C., Roy, F., Reszka, M., Colan, D. S., He, Z., Deacu, D., et al. :"Sea Ice forecast verification in the Canadian global ice ocean prediction system", Q. J. R. Meteorol. Soc. 142 (695), 659–671. doi: 10.1002/qj.2555 , 2016

Storto, A., S. Dobricic, S. Masina, and Di Pietro, P.: "Assimilating along-track altimetric observations through local hydrostatic adjustments in a global ocean reanalysis system", Mon. Wea. Rev. 139, 738-754, doi: 10.1175/2010MWR3350.1 ,2011.

Storto, A., Masina, S. and Dobricic, S.: "Estimation and Impact of Non-Uniform Horizontal Correlation Length-Scales for Global Ocean Physical Analyses", Journal of Atmospheric ad Ocean Technology, 31, 2330-2349, doi: 10.1175/JTECH-D-14-00042.1, 2014.

Storto, A., Masina, S. and Navarra, A. :"Evaluation of the CMCC eddy-permitting global ocean physical reanalysis system (C-GLORS, 1982–2012) and its assimilation components", Q.J.R. Meteorol. Soc., 142: 738-758, doi: 10.1002/qj.2673 , 2016.

Storto, A. and Masina, S. "C-GLORSv5: an improved multipurpose global ocean eddy-permitting physical reanalysis", Earth Syst. Sci. Data, 8, 679-696, doi: 10.5194/essd-8-679-2016 , 2016b.

Sun, J., Vecchi, G., Soden, B. :"Sea Surface Salinity Response to Tropical Cyclones Based on Satellite Observations", Remote Sens. 2021, 13, 420, doi: 10.3390/rs13030420 ,2021

Timmermann, R., H. Goosse, G. Madec, T. Fichefet, C. Ethé, and V. Duliére "On the representation of high latitude processes in the orcalim global coupled sea ice-ocean model", Ocean Modelling, 8:175–201, doi: 10.1016/j.ocemod.2003.12.009 , 2005.

Tonani, M., Pinardi, N., Fratianni, C., Pistoia, J., Dobricic, S., Pensieri, S., de Alfonso, M.; Nittis, K:"Mediterranean Forecasting System: Forecast and analysis assessment through skill scores", Ocean Sci. 5, 649–660, doi: 10.5194/os-5-649-2009 , 2009.

Tonani, M., Balmaseda, M., Bertino, L., Blockley, E., Brassington, G., Davidson, F., et al: "Status and future of global and regional ocean prediction systems", Journal of Operational Oceanography, 8(sup2), s201-s220, doi: 10.1080/1755876X.2015.1049892 , 2015.

U.S. Department of Commerce: 2-minute Gridded Global Relief Data (ETOPO2v2), National Oceanic and Atmospheric Administration, National Geophysical Data Center, doi:10.7289/V5J1012Q, 2006.

https://doi.org/10.5194/egusphere-2026-887
Preprint. Discussion started: 9 April 2026

Vincent, E. M., Lengaigne, M., Vialard, J., Madec, G., Jourdain, N. C. and Masson, S. : "Assessing the oceanic control on the amplitude of sea surface cooling induced by tropical cyclones", Journal of Geophysical Research Oceans, 117(C5), doi: 10.1029/2011jc007705 , 2012.

Wong, A. P. S., et al. :"Argo Data 1999–2019: Two Million Temperature-Salinity Profiles and Subsurface Velocity Observations From a Global Array of Profiling Floats", Frontiers in Marine Science, 7(700), doi: 10.3389/fmars.2020.00700Wond ,2020.

Yablonsky, R.M., Ginis, I. : "Impact of a Warm Ocean Eddy's Circulation on Hurricane-Induced Sea Surface Cooling with Implications for Hurricane Intensity", Mon Weather Rev. ,141(3): 997–1021, doi: 10.1175/MWR-D-12-00248.1 ,2012.

Yang, C., Masina, S. and Storto, A.: "Historical ocean reanalyses (1900–2010) using different data assimilation strategies", Q.J.R. Meteorol. Soc., 143: 479-493, doi: 10.1002/qj.2936 ,2017.

Zalesak, S. T.: "Fully multidimensional flux corrected transport for fluids", J. Comput. Phys., 31, 335-362, doi: 10.1016/0021-9991(79)90051-2 ,1979.

Zhang, H., He, H., Zhang, WZ. et al. :"Upper ocean response to tropical cyclones: a review", Geosci. Lett. 8, 1, doi: 10.1186/s40562-020-00170-8 ,2021